PCCP

Accepted Manuscript

ROYAL SOCIETY OF CHEMISTRY

www.rsc.org/pccp

Mechanism for the photo-reduction of poly(vinylpyrrolidone) to $HAuCl_4$ and the dominating saturable absorption of Au colloid

Guanghua Fan[a, b], Yanhua Han[b], Suilian Luo[c], Yutong Li[b], Shiliang Qu[b*], Qiang Wang[b], Renxi Gao[b], Minrui Chen[a], and Min Han[a*]

[a]*National Laboratory of Solid State Microstructures and Department of Materials Science and Engineering, Nanjing University, Nanjing 210093, China*

[b]*Department of Optoelectronic Science, Harbin Institute of Technology at Weihai, Weihai 264209, China*

[c]*School of Chemistry and Environment, South China Normal University, Guangzhou 510000, China*

[*]Corresponding author. E-mail: slqu@hit.edu.cn, sjhanmin@nju.edu.cn

Fax: 86-631-5687036

Abstract

Fabrication of Au nano-objects and the nonlinear optical properties of Au nano-objects are both research focus. In present work, Au nanoparticles with different mean size (18, 32, 42, and 70 nm) are controllably fabricated in ethanol by changing the concentration of poly(vinylpyrrolidone) (PVP) and $HAuCl_4$, as well as the power of continuous wave UV light at 365 nm. PVP acts as both the reducing and protective agent. The mechanism of photo-reduction of PVP to $HAuCl_4$ is proposed. PVP undergoes a series of chemical reactions which include the attack of hydrogen atom on the tertiary carbon atom at the α-position of nitrogen atom, production of hydroxyl, and chain scission. The hydroxyl combines with the hydrogen atom produced through the dissociation of $HAuCl_4$, which facilitates the decomposition of $HAuCl_4$. The fabrication mechanism of Au nanoparticles is discussed. The nonlinear absorptions of these Au nanoparticles are investigated, all of them exhibit saturable absorption, and the saturable absorption dominates the nonlinear absorption with increase of laser energy. The dominance of saturable absorption in the nonlinear absorption is due to the stronger single-photon absorbed intraband absorption from the ground state to the first excited state in the conduction band, the weaker excited state absorptions in the conduction band, and the weaker two-photon absorption from the *d* band to the conduction band.

1. Introduction

Fabrication of Au nano-objects has become a research focus. The simpler, safer, greener, and more effective method for fabrication of Au nano-objects is important and always pursued by researchers [1-3]. For fabrication of Au nano-object, $HAuCl_4$ is typically used as precursor and poly(vinylpyrrolidone) (PVP) is often used as protective agent. Usually, a reducing agent is needed to reduce Au(III) of $HAuCl_4$ to Au atom. C. E. Hoppe et al. reported the reduction of PVP for Au(III) of $HAuCl_4$ and fabrication of Au nanoparticles (NPs) by heating the mixed solution of $HAuCl_4$ and PVP [4]. Younan Xia et al. also reported the similar work [5]. The reducibility of PVP greatly simplifies the fabrication of Au NPs. In view of the biocompatibility of PVP, these works are meaningful for fabrication and application of Au NPs. However, these works are mainly performed in aqueous solution which is heated, the reducibility of PVP may be aroused by the elevated temperature [4-8]. The reducibility of PVP under light irradiation in organic solvent has less been concerned. In fact the fabrication of Au NPs in organic solvent is important, because this is a way leading to the fabrication of metal NPs doped organic films whose potential applications in optoelectronics devices have attracted increasing interests [9,10]. Ethanol can dissolve PVP and $HAuCl_4$, whose boiling point is low, the photo-fabrication of Au NPs in the presence of PVP in ethanol is a valuable choose. Although the photo-fabrication of metal NPs in water/ethanol in the presence of PVP is reported [11,14], the mechanism of photoreduction of PVP to $HAuCl_4$ and controllable photo-fabrication of Au NPs is further needed to be explored.

On the other hand, tremendous interests are focused on the nonlinear optical properties of Au NPs [15-25]. These properties depend on the intensity, wavelength, and pulse duration of laser, as well as the size, shape, and surface plasma resonance (SPR, the collective oscillation of the conduction electrons when the NPs are irradiated by the electromagnetic wave, which causes a peak in the optical extinction spectrum of the NPs) wavelength of Au NPs. There are also other factors such as NPs damage, solute migration, and bubbles of solution caused by the laser affect these

properties. It is revealed that Au NPs exhibit saturable absorption (SA) when the intensity of laser is low whereas reverse saturable absorption (RSA) when the intensity is high, usually, there is a changeover from SA to RSA as increase of the intensity [15,16,19]. It is also revealed that Au NPs exhibit RSA when the intensity is low whereas SA when the intensity is high, and there is a changeover from RSA to SA as increase of the intensity [22,23]. For the nonlinear optical properties of Au NPs, there are still many problems to be investigated. Among these problems, the domination of SA in the nonlinear absorption (NLA) of Au NPs, to the best of our knowledge, have not been reported.

In this work, a simple method for controllably fabricate Au NPs in ethanol by using PVP as both the reducing and protective agents is proposed. Under the irradiation of UV light, the photoreduction of PVP to Au(III) of $HAuCl_4$ takes place at room temperature. The sizes of Au NPs can be simply changed by changing the concentration of PVP and $HAuCl_4$, as well as the power of light. Au NPs with different mean size are fabricated, and the NLAs of these Au NPs are investigated by using Z-scan technique with femtosecond laser at 800 nm. Each sample exhibits SA, which does not change with increase of the laser energy. Mechanisms for the photoreduction of PVP to Au(III), the fabrication of Au NPs, and the domination of SA in the NLA are all discussed in detail.

2. Experimental details

The PVP and $HAuCl_4$ we used are purchased from Aladdin Industrial Corporation at Shanghai, the average molecular weight of this PVP is 5000 g/mol. $HAuCl_4$ and PVP are dissolved in ethanol. A quartz cuvette with $1\times1\times4$ cm^3 internal dimension is used to contain the liquid with liquid volume of 3 ml. A continuous wave UV lamp is used as light source, which operates at 365 nm and provides output powers of 40 or 20 watt. In our experiments, there are two different concentrations of $HAuCl_4$, four different concentrations of PVP, and two different powers of the UV light, which offer 6 schemes and produce 6 samples. These samples are labeled accordingly, as shown in the table 1. At room temperature, these samples are

irradiated by the UV light, as shown in the scheme 1. There is no stir in these samples. To evaluate the decomposition of $HAuCl_4$ and the formation of Au NPs, absorptive (or optical extinction) spectra of the as-processed samples are acquired by using a spectrophotometer (Shimadzu Corp., UV-1800) at different irradiation time. TEM characterization for Au NPs is carried out with a JEM 1400 transmission electron microscope (JEOL Ltd.). The Fourier transform infrared spectra of these samples are acquired by using a FT-IR spectrophotometer (Bruker). The ^1H NMR spectra are recorded by using a spectrometer (Varian, Avance III Ascend 500 HD). All ^1H NMR measurements are performed in $CDCl_3$ at room temperature, the frequency of the spectrometer is 500 MHz, and TMS is used as the internal standard. The NLA of Au NPs are investigated by using Z-scan technique. A regenerative amplified Ti:sapphire femtosecond laser system (Coherent Inc., Legend) is used to perform the Z-scan experiments. Laser pulses with wavelength of 800 nm, repetition rate of 200 Hz, and pulse duration of 120 fs are focused by a 20 cm focal length lens.

3. Results and discussions

3.1. The photochemical reactions of $HAuCl_4$ and PVP

The yellow solution of $HAuCl_4$ possesses a peak at 323 nm in the absorption spectrum when the concentration is low, which originates from the ligand-to-metal charge transfer band of $AuCl_4^-$ [26]. The peak becomes a much intensified platform at the range from 297 to 354 nm when the concentration of $HAuCl_4$ is increased to 2.33×10^{-3} mol/L, as shown in Fig. 1. With irradiation of the UV light, for the samples S11, S12, S22, S31, and S32, the platform narrows down and disappears, which indicates the decomposition of $HAuCl_4$, as shown in Fig. 2 (a), (b), (c), (d), and (e), respectively. And then a peak around 530 nm emerges and the height of the peak increases, which indicates the formation of Au NPs. It is noticeable that a sub-peak nearby the SPR peak of the sample S31 increases and then disappears with the irradiation time, as shown by a red arrow in Fig. 2 (e), which indicates the formation and precipitation of Au nanorods. The Au nanorods can be seen in the TEM image of the sample S31, as shown in the inset of Fig. 2 (e). And for the sample S35, the SPR

peak is faint although the irradiation time is long, as shown in Fig. 2 (f), which indicates that the formation of Au NPs in this sample is insignificant. The samples S11, S12, S22, and S32 are purple, and the sample S35 is almost colorless, all of them keep unchanged more than one year. Whereas the sample S31 is brown, in which the particles precipitate within several days.

To evaluate the role of PVP in decomposition of $HAuCl_4$ and formation of Au NPs, a solution of $HAuCl_4$ (2.33×10^{-3} mol/L) without PVP is also irradiated. The platform disappeared after a time which is much longer than that in the presence of PVP, and then a very faint SPR peak appears, as shown in Fig. 3. These experiments indicate that PVP dramatically facilitates the photodecomposition of $HAuCl_4$ and formation of Au NPs.

The photodecomposition of $HAuCl_4$ and formation of Au NPs in present work can be expressed as fellows [27,28]:

$$(HAu^{3+}Cl_4) \xrightarrow{hv} (HAu^{3+}Cl_4)^* \quad \text{(i)}$$

$$(HAu^{3+}Cl_4)^* \rightarrow (HAu^{2+}Cl_3) + Cl \quad \text{(ii)}$$

$$2(HAu^{2+}Cl_3) \xrightarrow{hv} (HAu^{3+}Cl_4) + (HAu^{1+}Cl_2) \quad \text{(iii)}$$

$$2(HAu^{1+}Cl_2) \xrightarrow{hv} (HAu^{2+}Cl_3) + H + Cl + Au^0 \quad \text{(iv)}$$

$$(HAu^{3+}Cl_4)^* + PVP \xrightarrow{hv} (HAu^{2+}Cl_3) + Cl + PVP^* \quad \text{(v)}$$

$$(HAu^{2+}Cl_3) + PVP \xrightarrow{hv} (HAu^{1+}Cl_2) + Cl + PVP^* \quad \text{(vi)}$$

$$(HAu^{1+}Cl_2) + PVP \xrightarrow{hv} Au^0 + H + 2Cl + PVP^* \quad \text{(vii)}$$

$$nAu^0 \longrightarrow (Au)_n \quad \text{(viii)}$$

The equation (i) describes the excitation of $HAuCl_4$ under the irradiation of UV light. When there is no PVP in the solution, the dissociation of $HAuCl_4$ and formation of Au atom are described by the equation (ii) to (iv), these reactions are very inefficient. And when there is PVP in the solution, the dissociation of $HAuCl_4$ and formation of Au atom are described by the equation (v) to (vii), these reactions are efficient for the promotion of PVP.

The photoreactions of PVP under irradiations of UV lights and various lasers are characterized by the FT-IR spectrum, transient grating method, size exclusion chromatography, and gas chromatography [29-32]. Herein the photoreaction of PVP in ethanol (4wt %) under the irradiation of UV light at 365 nm is characterized by the absorption spectrum, as shown in Fig. 4 (a). It can be seen that the absorbance from 230 nm to 600 nm decreases with the irradiation, which may be due to the scission of PVP chain caused by the irradiation. The photo of the sample S11 shot immediately after appearance of pink color is shown in Fig. 4 (b). It can be seen that the pink color is deep at the bottom of the solution (with continuation of the irradiation, the whole solution becomes pink colored subsequently), which indicates that Au NPs are initially formed at the bottom of the solution. This may also be due to the scission of PVP chain caused by the irradiation. Namely, with the scissions of PVP chain, the viscosity of the solution decreases, the as-formed Au NPs are settled in the bottom of the solution. For the samples S12, S22, S31, and S32, the settlements of initially formed Au NPs under the irradiation of UV light at 365 nm take place too. However, under the irradiation of UV light at 312 nm or 254 nm, the initially formed pink color of the solution is homogeneously distributed, as shown in Fig. 4 (b), which indicates that there is no settlement of the initially formed Au NPs.

The FT-IR spectra of PVP and $HAuCl_4$ before and after irradiation by UV light at 365 nm are characterized. In the FT-IR measurement, the solution is dropped onto the surface of thallium iodide wafer, and then the solution is blow-dryed, the remained film is analyzed. As can be seen from Fig. 4 (c), the peaks of $HAuCl_4$ are much weaker than that of PVP for the much lower concentration of $HAuCl_4$. Comparing to the PVP before irradiation, for the mixed solution of PVP and $HAuCl_4$ after irradiation, there is no peak disappears or emerges. For the PVP and $HAuCl_4$ mixed solution before and after irradiation, the heights of FT-IR peaks are shown in Fig. 4 (d). It can be seen that the peaks of the irradiated mixed solution of PVP and $HAuCl_4$ change obviously. The remarkable changes locate at 3449, 2953, 2921, 2880, 1681, 1423, 1286, 845, 734 and 649 cm^{-1}, which can be identified accordingly [33]. The peak at 3449 cm^{-1} is due to the OH stretch mode, which is easily affected by the

moisture because PVP is hygroscopic. The peak at 2953 and 2921 cm^{-1} is due to the CH_2 asymmetry and symmetry stretch mode of the pyrrolidone ring and PVP backbone, respectively. The peak at 2880 cm^{-1} is due to the C-H stretch mode. The peak at 1681 cm^{-1} is due to the C=O stretch mode. And the peak at 1423 and 1286 cm^{-1} is due to the CH_2 scissor and wag mode, respectively. The peak at 845 and 734 cm^{-1} is due to the C-C ring and C-C chain breathing mode, respectively. And the peak at 649 cm^{-1} is due to the N-C=O bend mode. The decrease and increase of peak height at 2953 and 1681 cm^{-1} may be due to the opening of pyrrolidone ring and scission of PVP chain, respectively [29-32].

The ^1H NMR tests of three samples are carried out at room temperature. A sample is PVP dissolved in $CDCl_3$, which is labeled as A0. The samples S11 and S22 are centrifuged after formation of Au NPs, the supernatants are dried in vacuum at room temperature, the as-formed films are dissolved in $CDCl_3$, which is labeled as S1 and S2, respectively. The ^1H NMR spectra of these samples are shown in Fig. 4 (e), the peaks are identified accordingly [34,35]. The decreases of peaks a and b of the samples S1 and S2 may indicate the scission of PVP chain. And the peaks c, d, and e of the samples S1 and S2 are different from that of the sample A0, which may indicate the opening of pyrrolidone ring. The end-group analysis of ^1H NMR spectroscopy is used to determine the molecular weight of PVP [36]. The test reveals that the average molecular weight of the reacted PVP in the sample S2 is smaller than 2000 g/mol, which indicates that the irradiation at 365 nm leads to the scission of PVP chain.

The photochemical reaction of PVP in water is investigated under the irradiation of UV light [29-32]. According to the commonly agreed reaction mechanism, the hydrogen atoms in PVP molecule are abstracted by certain radicals, which then leads to a series of reactions [29-32]. The radicals are produced through the photochemical reactions of chromophoric impurities in PVP, and/or other compound such as metal salt, hydrogen peroxide, and titanium dioxide particle that added into the solution. The photochemical reaction of PVP is less affected by the solvent. In present work the decomposition of $HAuCl_4$ produces chlorine atom which initiates the photochemical reaction of PVP. According to the experimental results and discussions mentioned

above, the reaction of PVP is proposed, which leads to the scission of PVP chain, as shown in scheme 2.

There are two carbon atoms in the α-position of the nitrogen atom of PVP molecule, either a secondary carbon atom or a tertiary one [31].

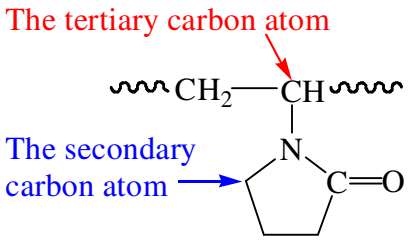

The first step of the photoreaction of PVP is hydrogen abstraction on the tertiary carbon atom at the α-position of nitrogen atom by chlorine atom. Then the macroradical is formed and reacts with oxygen, leading to peroxy radical that gives hydroperoxide by abstraction of a labile hydrogen atom (e.g. produced through the dissociation of $HAuCl_4$). The hydroperoxide is photochemically unstable, which is decomposed through the homolysis of the peroxide bond and gives hydroxyl radical and alkoxy radical. The alkoxy radical is decomposed through β-scission of the main chain of PVP, which decreases the average molecular weight of PVP [31]. And hydroxyl combines with the hydrogen atom produced through the dissociation of $HAuCl_4$. The decomposition of $HAuCl_4$ and PVP promotes each other, and PVP acts as the reducing agent. Although the FT-IR and ^1H NMR tests indicate the opening of pyrrolidone ring, the details are needed to be further investigated.

The SPR peak of the sample S11, S12, S22, and S32 is evaluated, and the optical extinction intensity at SPR peak wavelength is normalized, as shown in the inset of Fig. 2 (a), (b), (c), and (d), respectively. With irradiation the narrow down of SPR peak indicates the narrow down of size distribution of Au NPs. For the samples S11, S12, S22, and S32, the time evolutions of SPR peak wavelength are shown in Fig. 5 (a), (b), (c), and (d), respectively. The increase and plateau structure in the evolution curve indicates that the mean sizes of Au NPs increase quickly at a early stage and then the increase slows down [37]. Namely, the mean sizes of Au NPs are saturated and no longer able to increase at last. For the samples S11, S12, S22, and S32, the time evolutions of the optical extinction intensity at SPR peak wavelength are also

shown in Fig. 5 (a), (b), (c), and (d), respectively. The increase of the optical extinction intensity at the SPR peak indicates the increase of the large sized Au NPs (there is no SPR for the Au particle smaller than 2 nm [38,39]). This also indicates the continuous formation of Au nuclei. However, the amount of these continuously formed nuclei decreases with the irradiation time. Otherwise, the later formed nuclei should be seen in the TEM images. Namely, the absence of very small Au NPs in the TEM images indicates that the Au nuclei are mainly formed at the early stage, all the saturated sized Au NPs grow from these earlier formed nuclei, as shown in Fig. 6.

The TEM image of Au NPs in the sample S11, S12, S22, and S32 is shown in Fig. 6 (a), (b), (c), and (d), respectively. The corresponding size distribution histograms are shown as the insets. The average size of Au NPs in the samples S11, S12, S22, and S32 is 18, 70, 32, and 42 nm, respectively. Comparing to the NPs in the sample S11, the NPs in the sample S12 are much larger for the lower irradiation power; and the NPs in the sample S22 are larger for the higher concentration of $HAuCl_4$; and the NPs in the sample S32 are larger for the lower concentration of PVP. Namely, the controllable fabrication of Au NPs can be achieved by changing the irradiation power of the UV light and the concentration of $HAuCl_4$ and PVP. The reason is that the high concentration of $HAuCl_4$ provides more Au atoms to form larger Au NPs. And the low concentration of PVP less restrains the thermal motion of Au atoms, so a particle can "absorb" more atoms to form a lager particle. In the case of low irradiation power, a slow release of Au atoms through the decomposition of $HAuCl_4$ leads to a less amount of Au nuclei initially. These nuclei and the successive arriving Au atoms experience competitions in growing up into NPs or nuclei. Comparing to an Au atom, an Au nucleus possesses a larger absorption cross section, so the successive arriving atoms tend to combine with the initially formed nuclei rather than combine with other atoms. Therefore these initially formed nuclei experience a more sufficient growth through the absorption of the slow arriving but long term sustaining Au atoms and grow into large Au NPs. The TEM image of Au NPs in the sample S31 is shown in the inset of Fig. 2 (e), there are many nanorods, which is unlike to that of the sample S11, S12, S22, and S32, and also unlike to the

results of previously reported works in which the solution is heated and nanorods are formed with low concentration of PVP [4,40]. The difference of formation mechanisms of Au NPs among these results is needed to be explored. And for the sample S35, there is little Au NPs can be observed because the rather low concentration of PVP can not reduce $HAuCl_4$ to Au atoms to form Au NPs.

3.2. The nonlinear absorption of Au colloids

The sample S11, S12, S22, and S32 is filled in a glass cell with inner optical path of 2 mm, the linear transmittance of the sample at 800 nm is 80%, 71%, 74%, and 73%, respectively. The open aperture (OA) Z-scan experiment of each sample is performed, each transmittance curve exhibits a peak which indicates the SA [41], as shown in Fig. 7. In a wide range of intensity (from 6.65 to 100 GW/cm^2), the NLA of each sample is dominated by the SA, and there is no change from SA to RSA. The OA Z-scan experiments of the supernatants of these samples are also performed and no NLA can be found, which indicates that the Au NPs exhibit SA.

The NLA of Au NPs includes the interband absorption from the *d* band to conduction band and the intraband absorption in the conduction band, as shown by the cyan and orange arrows in Fig. 8 (a), respectively. The interband absorption at 800 nm (1.55 eV) is two-photon absorption (TPA) due to an energy gap between the *d* band and conduction band (2.4 eV) [42]. The interband absorption takes place at the *L* point of Brillouin zone. The intraband absorption includes a series of single-photon absorptions (SPAs) which take place from the ground (or lower excited) state to the first (or higher) excited state. All the excited conduction band electrons ultimately relax to the ground state in the conduction band. Since the effective mass of the *d* band electron is larger than that of conduction band electron, the *d* band electron is less easily be excited comparing to that of conduction band electron [17]. Beyond that, the behavior of the excited *d* band electron in the conduction band is similar to that of conduction band electron. Note that all the excited *d* band electrons ultimately relax to the *d* band rather than the conduction band.

The NLA is described as possible electron transitions that take place in a

five-level model, as shown in Fig. 8 (b). In Fig. 8 (b), the states in the conduction band are drown as red horizontal lines. The ground state, the first, second, and third excited state is denoted as C_0, C_1, C_2, and C_3, respectively. The *d* band is drown as a blue horizontal line and denoted as D. According to the discussions mentioned above, the transitions and relaxations of conduction band electrons and the transitions and relaxations of *d* band electrons are independent and therefore can be divided, as shown by the dotted lines in the red horizontal lines.

The transitions and relaxations of the conduction band electrons are shown by the red arrows in the Fig. 8 (b). A part of electrons in the ground state C_0 are excited to the first excited state C_1 through an SPA process. The electrons in the state C_1 may relax back to the state C_0 by a nonradiative transition, or undergo an SPA process and excite to the second excited state C_2. The electrons in the state C_2 may relax back to the state C_1 by a nonradiative transition, or undergo an SPA process and excite to the third excited state C_3. The transitions and relaxations of conduction band electrons can be described by the rate equations

$$\frac{dN_{C0}}{dt} = -\frac{\sigma_0 I N_{C0}}{\hbar\omega} + \frac{N_{C1}}{\tau_{10}}, \tag{1}$$

$$\frac{dN_{C1}}{dt} = \frac{\sigma_0 I N_{C0}}{\hbar\omega} - \frac{N_{C1}}{\tau_{10}} - \frac{\sigma_1 I N_{C1}}{\hbar\omega} + \frac{N_{C2}}{\tau_{21}}, \tag{2}$$

$$\frac{dN_{C2}}{dt} = \frac{\sigma_1 I N_{C1}}{\hbar\omega} - \frac{N_{C2}}{\tau_{21}}, \tag{3}$$

$$\alpha_C = \sigma_0 N_{C0} + \sigma_1 N_{C1} + \sigma_2 N_{C2}, \tag{4}$$

where N_{C0}, N_{C1}, and N_{C2} are the number densities of conduction band electrons in the states C_0, C_1, and C_2, respectively. σ_0, σ_1, and σ_2 are the absorption cross sections of the states C_0, C_1, and C_2, respectively. τ_{10} and τ_{21} are the relaxation times of the states C_1 and C_2, respectively. Since the lifetime of the state C_3 is very short ($\tau_{32}\approx 0$), so the number density of electrons in this state can be neglected ($N_{C3}\approx 0$). $\hbar\omega$ is the photon energy of the laser. α_C is the absorption coefficient of the conduction band electrons.

The transitions and relaxations of the *d* band electrons are shown by the blue

arrows in the Fig. 8 (b). A part of electrons in the state D are excited to the state C_0 through a TPA process. The *d* band electrons in the state C_0 may relax back to the state D by a nonradiative transition, or undergo an SPA process and excite to the first excited state C_1. The *d* band electrons in the state C_1 may relax back to the state C_0 by a nonradiative transition, or undergo an SPA process and excite to the second excited state C_2. The *d* band electrons in the state C_2 may relax back to the state C_1 by a nonradiative transition, or undergo an SPA process and excite to the third excited state C_3. The transitions and relaxations of *d* band electrons can be described by the rate equations

$$\frac{dN_D}{dt} = -\frac{\beta I^2 N_D}{2\hbar\omega} + \frac{N'_{C0}}{\tau_{0D}}, \tag{5}$$

$$\frac{dN'_{C0}}{dt} = \frac{\beta I^2 N_D}{2\hbar\omega} - \frac{N'_{C0}}{\tau_{0D}} - \frac{\sigma_0 I N'_{C0}}{\hbar\omega} + \frac{N'_{C1}}{\tau_{10}}, \tag{6}$$

$$\frac{dN'_{C1}}{dt} = \frac{\sigma_0 I N'_{C0}}{\hbar\omega} - \frac{N'_{C1}}{\tau_{10}} - \frac{\sigma_1 I N'_{C1}}{\hbar\omega} + \frac{N'_{C2}}{\tau_{21}}, \tag{7}$$

$$\frac{dN'_{C2}}{dt} = \frac{\sigma_1 I N'_{C1}}{\hbar\omega} - \frac{N'_{C2}}{\tau_{21}}, \tag{8}$$

$$\alpha_D = \beta I N_D + \sigma_0 N'_{C0} + \sigma_1 N'_{C1} + \sigma_2 N'_{C2}, \tag{9}$$

where N_D is the number density of the *d* band electrons that can be excited to the conduction band. N'_{C0}, N'_{C1}, and N'_{C2} are the number densities of *d* band electrons excited to the states C_0, C_1, and C_2, respectively. Similarly, the number density of *d* band electrons in the state C_3 is neglected. τ_{0D} is the relaxation time of the *d* band electrons from the state C_0 to D. β is the TPA coefficient from the state D to C_0. α_D is the absorption coefficient of the *d* band electrons.

The absorption of the sample is described by the Beer's law equation

$$\frac{dI}{dz'} = -(\alpha_C + \alpha_D) I, \tag{10}$$

where z' is the penetration depth of the laser pulse into the sample. In the OA Z-scan experiment, the intensity *I* varies with z, r, and t as

$$I(z,t) = I_0 \frac{\omega_0^2}{\omega^2(z)} \exp\left\{-\left[\frac{2r^2}{\omega^2(z)}\right]\right\} \exp\left[-\left(\frac{t}{\tau}\right)^2\right], \quad (11)$$

where $\omega(z) = \omega_0\left[1+\left(z/z_0\right)^2\right]^{1/2}$ is the beam radius at z, z is the sample position away from the focus of the laser beam, $z_0 = \pi\omega_0^2/\lambda$ is the diffraction length of the beam, ω_0 is the beam radius at the focus, and I_0 is the on-axis peak irradiance at the focus and can be calculated from $I_0 = 2E/\left(\pi^{3/2}\omega_0^2\tau\right)$, E is the energy of the laser pulse, and τ is the pulse duration of the laser.

To fit the experimental data of these samples, the corresponding parameters are selected. The relaxation times of the states relate to the ultrafast dynamics of Au NPs. For Au NPs (with diameter of 48 nm), under the excitation of low intensity, the conduction band electrons that absorbed the photon energy are excited, which collide with the unexcited electrons and leads to the thermalization of the electron gas that possesses the energy nearby the Fermi level. The thermalization of electron gas is described by the electron-electron interaction time ($\tau_{e\text{-}e}$), which is about 450 fs [43]. And then the thermalized electron gas interacts with the lattice of Au particle, leading to the thermalization of the particle, the electron-phonon interaction time ($\tau_{e\text{-}ph}$) is about 1.7 ps. At last the Au NPs interact with the solvent through the phonon-phonon interaction, which heats the solvent by consuming the thermal energy of Au NPs, the phonon-phonon interaction time ($\tau_{ph\text{-}ph}$) is about 90 ps. Obviously, the $\tau_{e\text{-}e}$ can be reasonably viewed as τ_{10}. For Au NPs, the $\tau_{e\text{-}e}$ is found to be size independent in the diameter range from 9 to 48 nm (~500 fs) [43]. For Au film with thickness of 300 nm, $\tau_{e\text{-}e}$ is found to 600 fs [44]. So for Au NPs, the $\tau_{e\text{-}e}$ is considered to be size independent. The τ_{10} of the samples S11, S12, S22, and S32 can be all reasonably assigned to be 500 fs. As far as we know, the relaxation time of the second and higher excited states in the conduction band (i.e. τ_{21} and τ_{32}) are not clear. However τ_{21} and τ_{32} should be much shorter than τ_{10}, and τ_{32} should be much shorter than τ_{21}. These are reasonable because the higher excited state typically possesses a shorter relaxation time. To fit the experiment data, τ_{21} and τ_{32} are assumed to be also size independent and assigned

to be 20 and 0 fs, respectively. The τ_{0D} is the relaxation time of the *d* band electrons from the state C_0 to D, which relates to the recombination of the *d* band electrons and holes. Efforts are made to investigate this problem. The τ_{0D} is assumed to be size independent and longer than the $\tau_{e\text{-}e}$, which is assigned to be 800 fs for each sample.

The molar concentration of Au NPs in the sample S11, S12, S22, and S32 is 3×10^{-5}, 5×10^{-7}, 1×10^{-5}, and 2×10^{-6} mol/*L*, respectively. The linear absorption cross section σ_0 of an Au NP can be deduced from the linear absorption coefficient $\alpha_0=N\sigma_0$, where $\alpha_0=-\ln T/L$ with *T* the linear optical transmittance, *L* the thickness of the colloid, and *N* the number of Au NPs in an unit volume of colloid. According to the method reported in the previous literatures [22,23,45,46], the TPA coefficients of the samples S11, S12, S22, and S32 are calculated to be 1.3×10^{-14}, 1×10^{-14}, 1.5×10^{-14}, and 1.5×10^{-14} m/W, respectively. The TPA coefficient β of an Au NP in the samples S11, S12, S22, and S32 is calculated, as listed in the table 2. The conduction band electrons travel freely inside Au NPs, which can be all excited. So N_{C0} is assigned to be 5.9×10^{22} cm^{-3} [47]. Accordingly N_{C1} and N_{C2} before the excitation is 0 and 0, respectively. The occupied density of state of 5*d* band electrons of Au NP (with electron configuration of $5d^{10}6s^1$) extends from 2 to 8 eV below the Fermi level [48]. The 5*d* electrons far below the Fermi level can not contribute to the interband TPA at 800 nm. So N_D is assigned to be $3\times N_{C0}(-\infty)$, i.e., 30% of the number density of 5*d* band electrons. The beam radius at the focus is 20 μm. The experimental data are fitted with the equations (1) to (11), as shown in the Fig. 7. The fitting parameters are listed in the table 2. For each sample, the σ_1 is smaller than the σ_0, which may be viewed as a regularity. However, there is no similar regularity between the σ_2 and σ_0. More importantly, in fact, the NLA of the sample is decided by the sum of α_C and α_D. If the sum of α_C and α_D decreases (increases) with the increasing intensity, the NLA is SA (RSA). In this sense, the irregularity between the σ_2 and the σ_0 can be understood and ignored. These discussions can be verified by selecting the sample S11 as an example, as discussed below.

For the sample S11, with the irradiation of a laser pulse, the conduction band electrons in the states C_0 decrease initially and increase afterwards, and the electrons

in the states C_1 and C_2 increase initially and decrease afterwards, as shown in Fig. 9 (a). Since N_{C0} is larger than N_{C1} and much larger than N_{C2}, so the absorption coefficient of the conduction band electrons $\alpha_C = \sigma_0 N_{C0} + \sigma_1 N_{C1} + \sigma_2 N_{C2}$ decreases initially and increases afterwards. As a whole, α_C decreases with the irradiation of a laser pulse, as shown by the red line in Fig. 9 (c). With the irradiation of a laser pulse, the *d* band electrons in the state D decrease initially and increase afterwards, and the *d* band electrons that excited to the states C_0, C_1, and C_2 increase initially and decrease afterwards, as shown in Fig. 9 (b). For the *d* band electrons, since their TPA is stronger than their NLA in the conduction band, so their absorption coefficient $\alpha_D = \beta I N_D + \sigma_0 N_{C0}^{'} + \sigma_1 N_{C1}^{'} + \sigma_2 N_{C2}^{'}$ is mainly decided by the TPA, which increases initially and decreases afterwards, as shown by the black line in Fig. 9 (c). However, as a whole, the total absorption coefficient is mainly contributed by the α_C, which decreases with the irradiation of a laser pulse, as shown by the blue line in Fig. 9 (c). So the NLA of the sample S11 is dominated by the SA. In addition, for the sample with $\sigma_0 > \sigma_1$ and $\sigma_0 > \sigma_2$, similar analysis reveals that the NLA is also dominated by the SA. In a word, for each sample, the dominance of SA in the NLA is due to the stronger SPA from C_0 to C_1, the weaker excited state absorptions in the conduction band which is due to the short relaxation time and small absorption cross section, as well as the weaker TPA from the *d* band to conduction band.

In addition to the NLA, other factors that influence the OA Z-scan transmittance should be also noticed. These factors include the fragmentation of NPs, solute migration, and nonlinear optical scattering, which enhance as the increasing intensity. The fragmentation of metal NPs is a result of photoejection of electrons that are caused by the multi-photon absorption, which decreases the transmittance of the sample [49]. In present work, each sample with volume of 0.2×1×1 cm^3 is placed at the focus of Z-scan experiment, at which the peak intensity is 100 GW/cm^2. This intensity is equal to the maximum intensity that used in the Z-scan experiment. The irradiation is persisted for 2 hours with the repetition rate of laser pulse is 200 Hz. The TEM image of Au NPs in the irradiated sample 11 is shown in Fig. 10. It can be seen

that the morphology changes are insignificant, as pointed out by the arrows. The morphology changes of other samples are also insignificant. These results rule out the effect of fragmentation of NPs to the OA Z-scan transmittance. As introduced previously, the laser heats the electron gas which interacts with the lattice of Au particle, leading to the thermalization of the particle. This process is almost nonradiative, so large amount of excess energy of Au NPs are converted from the energy that absorbed from the laser [43,50,51]. The highly concentrated excess energy leads to an "explosion" in the colloid [50,51], which pushes the Au NPs laterally outward from the center of the laser beam, leading to the migration of Au NPs. The migration causes the concentration gradient of Au NPs in the colloid. If the concentration gradient caused by a laser pulse sustains until the arrival of the next pulse, the absorption of the next pulse will be weakened, so the transmittance increases. This cumulative effect becomes more severe as the sample is moved to the focus of Z-scan experiment [50-52]. In present work the viscous colloid matches these conditions. So the effect of Au NPs migration to the OA Z-scan transmittance may not be ignored, however the details are needed to be further investigated. The nonlinear optical scattering in liquid is caused by the bubble which is caused by the heated particle. The scattering decreases the transmittance of laser. However, the pulse duration of the femtosecond laser is much shorter than the time for forming a bubble, so the scattering in present works can be reasonably neglected.

4. Conclusions

In present work, Au NPs with different mean size are controllably fabricated in ethanol by changing the concentration of PVP and $HAuCl_4$, as well as the power of UV light. The mechanism of photo-reduction of PVP to $HAuCl_4$ under the irradiation of UV light is proposed. PVP undergoes a series of chemical reactions which include the attack of hydrogen atom on the tertiary carbon atom at the α-position of nitrogen atom, production of hydroxyl, and chain scission. The hydroxyl combines with the hydrogen atom produced through the dissociation of $HAuCl_4$, which facilitates the decomposition of $HAuCl_4$. The fabrication mechanism of Au NPs is discussed. The

NLA of Au NPs with four different mean sizes are investigated, all of them exhibit SA, and the SA dominates the NLA with the increase of laser energy. The dominance of SA in the NLA is due to the stronger single-photon absorbed intraband absorption from the ground state to the first excited state in the conduction band, the weaker excited state absorptions in the conduction band, and the weaker two-photon absorption from the *d* band to conduction band.

Acknowledgments

This research is partly supported by the Natural Scientific Research Innovation Foundation in Harbin Institute of Technology (Project HIT. NSRIF. 2014140), and the Project of Shandong Province Higher Educational Science and Technology Program (Project J14LJ54), as well as the National Natural Science Foundation of China (Grant Nos. 11374077, 11304065, 11274082, 51171077, 11574064). Guanghua Fan thanks professor Changlu Gao and doctor Xinbo Wang for their helpful discussions.

References

[1] P. Quaresma, L. Soares L. Contar, A. Miranda, I. Osório, P. A. Carvalho, R. Franco and E. Pereira, *Green Chem.*, 2009, 11, 1889

[2] H. Wei, Z. Wang, J. Zhang, S. House, Y. Gao, L. Yang, H. Robinson, L. H. Tan, H. Xing, C. Hou, I. M. Robertson, J. Zuo and Y. Lu, *Nat. Nanotechnol.*, 2011, 6, 93

[3] B. Tangeysh, K. M. Tibbetts, J. H. Odhner, B. B. Wayland and R. J. Levis, *J. Phys. Chem. C*, 2013, 117, 18719

[4] C. E. Hoppe, M. Lazzari, I. Pardiñas-Blanco and M. A. López-Quintela, *Langmuir*, 2006, 22, 7027

[5] Y. Xiong, I. Washio, J. Chen, H. Cai, Z. Li, and Y. Xia, *Langmuir*, 2006, 22, 8563

[6] I. Pardiñas-Blanco, C. E. Hoppe, Y. Piñeiro-Redondo, M. A. López-Quintela, and J. Rivas, *Langmuir*, 2008, 24, 983

[7] B. Lim, P. H. C. Camargo, and Y. Xia, *Langmuir*, 2008, 24, 10437

[8] L. Kemal, X. C. Jiang, K. Wong, and A. B. Yu, *J. Phys. Chem. C*, 2008, 112, 15656

[9] X. Liu, K. Matsumura, Y. Tomita, K. Yasui, K. Kojima, and K. Chikama, *J. Appl.*

Phys., 2010, 108, 073102

[10] T. He, C. Wang, X. Pan, and Y. Wang, *Phys. Lett. A*, 2009, 373, 592

[11] M. Harada, and H. Einaga, *Langmuir*, 2007, 23, 6536

[12] Masafumi Harada, Koichi Okamoto, and Masahide Terazima, *J. Colloid Interf. Sci.*, 2009, 332, 373

[13] Y. Nakazato, K. Taniguchi, S. Ono, T. Eitoku and K. Katayama, *Phys. Chem. Chem. Phys.*, 2009, 11, 10064

[14] N. Maeda, T. Eitoku, Y. Ikezoe and K. Katayama, *Phys. Chem. Chem. Phys.*, 2012, 14, 200

[15] R. Philip and G. R. Kumar, *Phys. Rev. B*, 2000, 62,13160

[16] S. Qu, C. Zhao, X. Jiang, G. Fang, Y. Gao, H. Zeng, Y. Song, J. Qiu, C. Zhu and K. Hirao, *Chem. Phys. Lett*., 2003, 368, 352

[17] S. Qu, Y. Zhang, H. Li, J. Qiu and C. Zhu, *Opt. Mater*., 2006, 28, 259

[18] R. A. Ganeev, M. Suzuki, M. Baba, M. Ichihara and H. Kuroda, *J. Appl. Phys*., 2008, 103, 063102

[19] Y. H. Lee, Y. Yan, L. Polavarapu and Q. Xu, *Appl. Phys. Lett*., 2009, 95, 023105

[20] X. Liu, K. Matsumura, Y. Tomita, K. Yasui, K. Kojima and K. Chikama, *J. Appl. Phys*., 2010, 108, 073102

[21] R. A. Ganeev, G. S. Boltaev, R. I. Tugushev and T. Usmanov, *Appl. Phys. B*, 2010, 100, 571

[22] K. Wang, H. Long, M. Fu, G. Yang and P. Lu, *Opt. Express*, 2010, 18, 13874

[23] K. Wang, H. Long, M. Fu, G. Yang and P. Lu, *Opt. Lett*., 2010, 35, 1560

[24] Z. Chen, H. Dai, J. Liu, H. Xu, Z. Li, Z. Zhou and J. Han, *Opt. Express*, 2013, 21, 17568

[25] O. Sánchez-Dena, P. Mota-Santiago, L. Tamayo-Rivera, E. V. García-Ramírez, A. Crespo-Sosa, A. Oliver and J. -A. Reyes-Esqueda, *Opt. Mater. Express*, 2014, 4, 92

[26] S. Yang, Y. Wang, Q. Wang, R. Zhang and B. Ding, *Colloid Surface A*, 2007, 301, 174

[27] K. Kurihara, J. Kizling, P. Stenius and J. H. Fendler, *J. Am. Chem. Soc*., 1983,

105, 2574

[28] S. Eustis, H. Hsu and M. A. El-Sayed, *J. Phys. Chem. B*, 2005, 109, 4811

[29] H. Kaczmarek, A. Kamińska, M. Swiatek and J. F. Rabek, *Die Angewandte Makromolekulare Chemie*, 1998, 261/262, 109

[30] S. Horikoshi, H. Hidaka and N. Serpone, *J. Photoch. Photobio. A*, 2001, 138, 69

[31] F. Hassouna, S. Therias, G. Mailhot and J. Gardette, *Polym. Degrad. Stabil.*, 2009, 94, 2257

[32] F. Hassounaa, G. Mailhota, S. Morlat-Thérias and J. Gardette, *J. Photoch. Photobio. A*, 2011, 218, 239

[33] Y. Borodko, S. E. Habas, M. Koebel, P. Yang, H. Frei and G. A. Somorjai, *J. Phys. Chem. B*, 2006, 110, 23052

[34] B. Sesta, A. L. Segre, A. D'Aprano and N. Proietti, *J. Phys. Chem. B*, 1997, 101, 198

[35] B. Sesta, A. D'Aprano, A. L. Segre and N. Proietti, *Langmuir*, 1997, 13, 6612

[36] P. Zhang, X. Zhong, Y. Chai, and Y. Liu, *Colloid Polym. Sci.*, 2008, 286, 1135

[37] K. Mougin, Z. Zheng, N. Piazzon, E. Gnecco and H. Haidara, *J. Colloid Interf. Sci.*, 2009, 333, 719

[38] O. R. Miranda and T. S. Ahmadi, *J. Phys. Chem. B*, 2005, 109, 15724

[39] Y. Lu, M. Dasog, A. F. G. Leontowich, R. W. J. Scott, and M. F. Paige, *J. Phys. Chem. C*, 2010, 114, 17446

[40] Y. Yang, S. Matsubara, L. Xiong, T. Hayakawa, and M. Nogami, *J. Phys. Chem. C*, 2007, 111, 9095

[41] M. Sheik-Bahae, A. A. Said, T. H. Wei, D. J. Hagan and E. W. Van Stryland, *IEEE J. Quantum Elect.*, 1990, 26, 760

[42] L. Yang, D. H. Osborne, R. F. Haglund, Jr., R. H. Magruder, C. W. White, R. A. Zuhr, H. Hosono, *Appl. Phys. A*, 1996, 62, 403

[43] S. Link, M. A. El-Sayed, *J. Phys. Chem. B*, 1999, 103, 8410

[44] W. S. Fann, R. Storz, H. K. Tom, and J. Boker, *Phys. Rev. Lett.*, 1992, 68, 2834

[45] R. A. Ganeev, A. I. Ryasnyansky, A. L. Stepanov, T. Usmanov, *Phys. Stat. Sol. B*, 2004, 241, R1

[46] P. Thomas, P. Sreekanth, and K. E. Abraham, *J. Appl. Phys.*, 2015, 117, 053103

[47] K. Lee, and M. A. El-Sayed, *J. Phys. Chem. B*, 2006, 110, 19220

[48] B. Balamurugan, and Toshiro Maruyama, *Appl. Phys. Lett.*, 2005, 87, 143105

[49] P. V. Kamat, M. Flumiani, and G. V. Hartland, *J. Phys. Chem. B*, 1998, 102, 3123

[50] T. Wei, C. Wang, T. Wu, C. Chen, X. Li, T. Huang, S. Yang and T. Wei, *J. Chem. Phys*., 2004, 120, 8031

[51] C. Chang, Y. Li, C. Chen, L. Lee, J. Tang, C. Wang, C. Leu, T. Wei, T. Huang and Y. Song, *J. Chem. Phys*., 2009, 130, 024511

[52] Y. Gao, W. Wu, D. Kong, L. Ran, Q. Chang and H. Ye, *Physica E*, 2012, 45, 162

Table 1 The compositions of the samples before irradiation; and the irradiation schemes of the experiments as well as the mean size of the as-produced Au NPs.

Sample	concentration of $HAuCl_4$ ($\times 10^{-3}$ mol/L)	concentration of PVP (wt%)	powers of the UV light (watts)	mean size of the NPs (nm)
S11	2.33	3.2	40	18
S12	2.33	3.2	20	70
S22	4.66	3.2	40	32
S31	2.33	6.4	40	--
S32	2.33	1.6	40	42
S35	2.33	0.13	40	--

Table 2 The fitting parameters of the rate equations.

The fitting parameters.	S11	S12	S22	S32
σ_0 of an Au NP, ($\times 10^{-21}$ m^{-2})	6.2	570	25	130
σ_1 of an Au NP, ($\times 10^{-21}$ m^{-2})	1.55	559	5.2	86.7
σ_2 of an Au NP, ($\times 10^{-20}$ m^{-2})	3.72	21	6.5	6.5
β of an Au NP, ($\times 10^{-37}$ m/W)	7.2	330	25	125

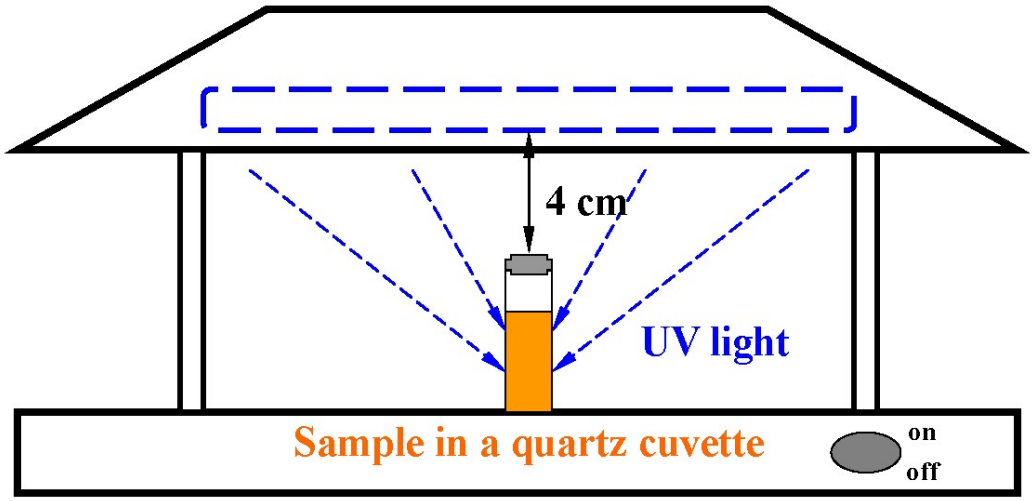

Scheme 1 The schematic of experimental setup.

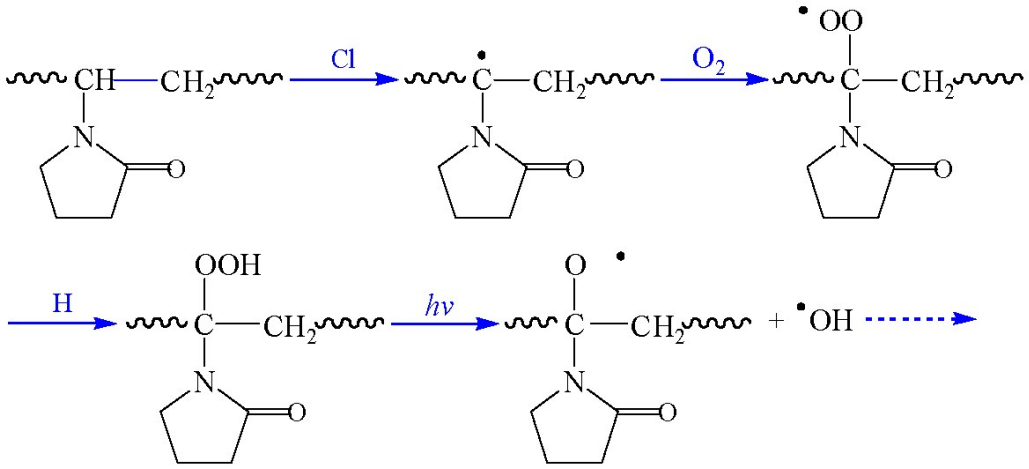

Scheme 2 The photoreaction of PVP under irradiation of UV light at 365 nm.

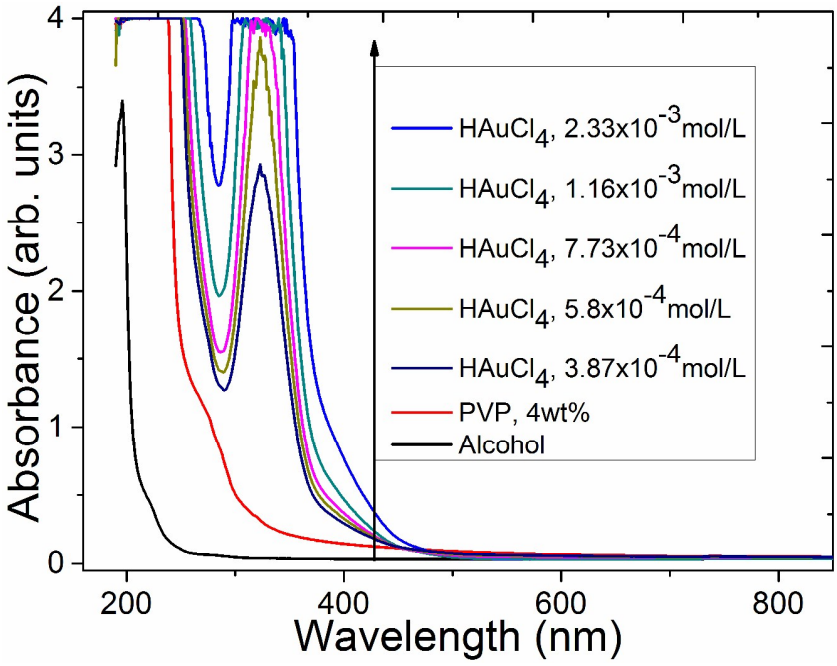

Fig. 1 The absorption spectra of ethanol, PVP in ethanol, and HAuCl4 in ethanol with different concentrations.

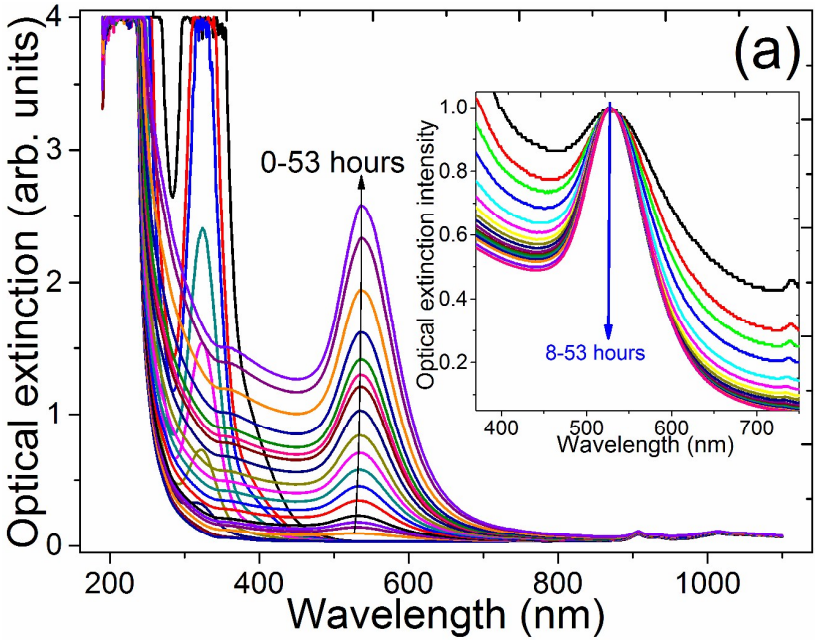

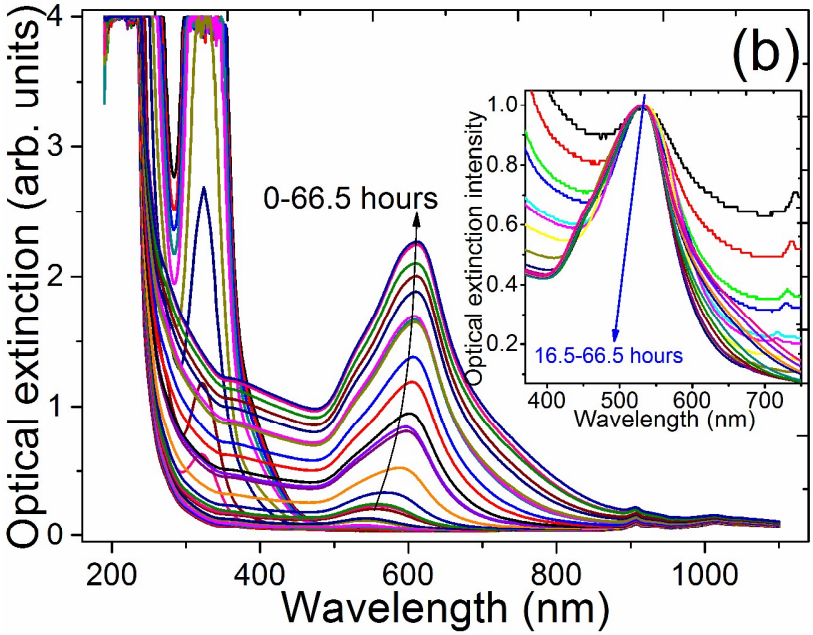

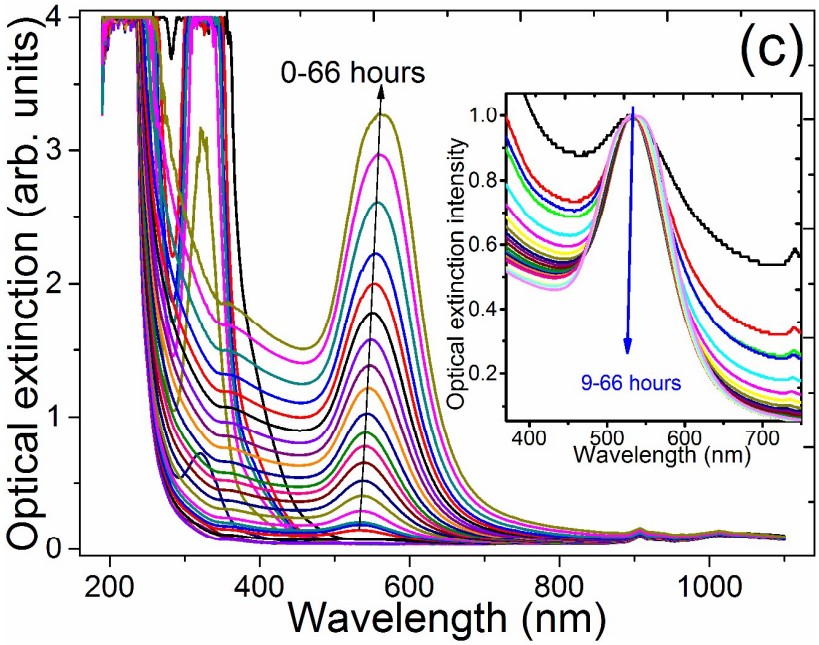

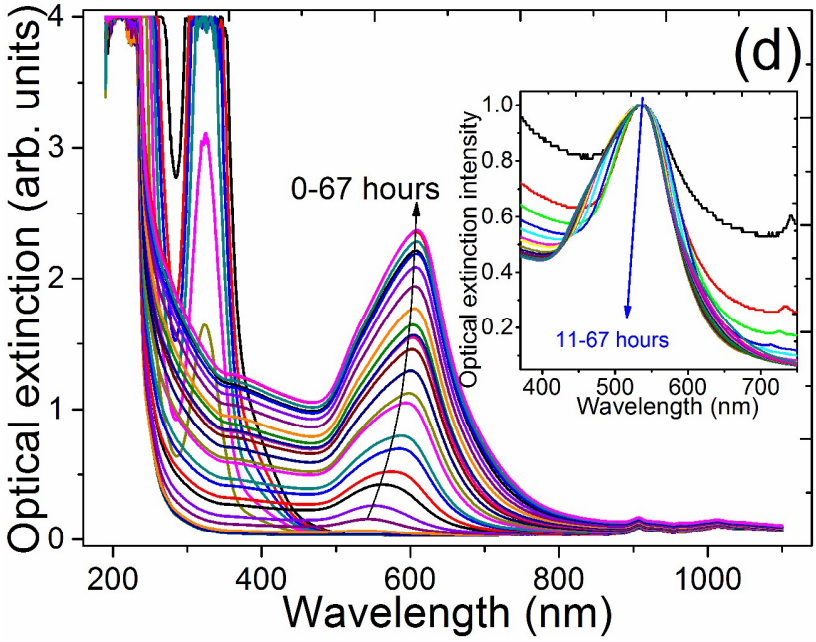

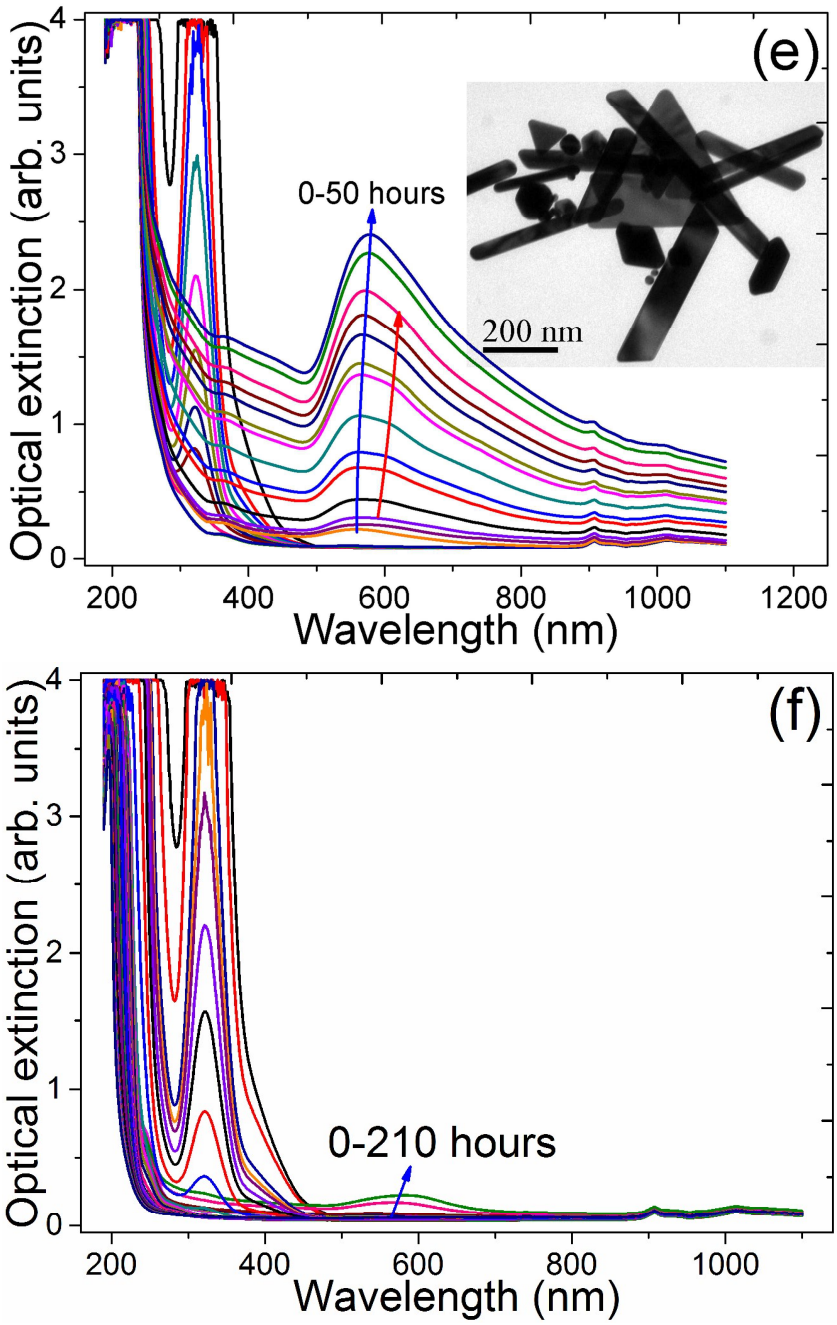

Fig. 2 The absorption (or optical extinction) spectra of the samples irradiated by UV light at 365 nm. (a) sample 11, (b) sample 12, (c) sample 22, (d) sample 32, (e) sample 31, (f) sample 35; the inset in (a), (b), (c), and (d) is the corresponding optical extinction spectra at the SPR of the as-producing Au NPs, which are normalized at the SPR peak wavelength. The inset in (e) is the TEM image of Au NPs in the sample 31.

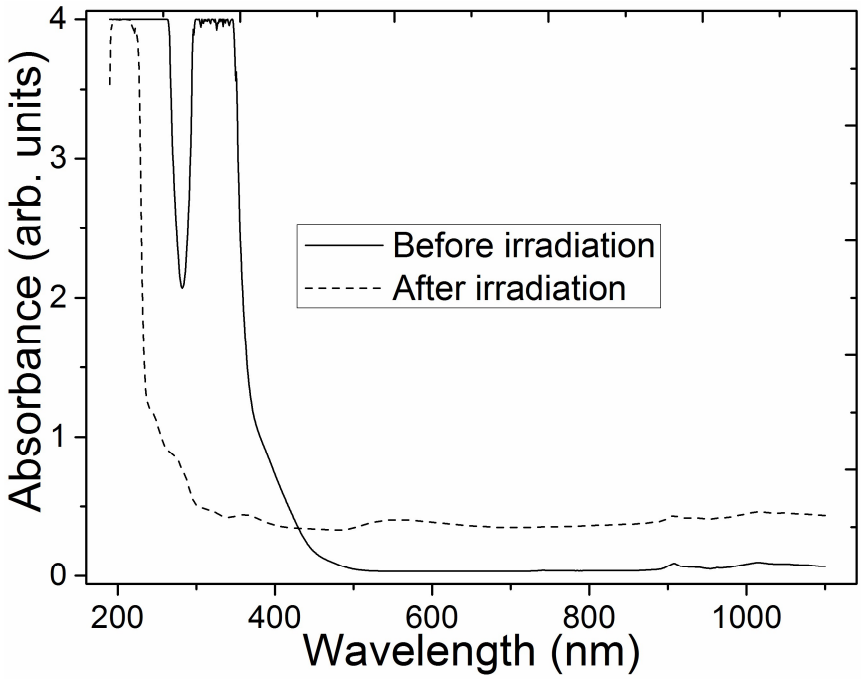

Fig. 3 The absorption spectra of $HAuCl_4$ in ethanol in absence of PVP, black and blue line is the spectrum before and after irradiation by UV light at 365 nm, respectively.

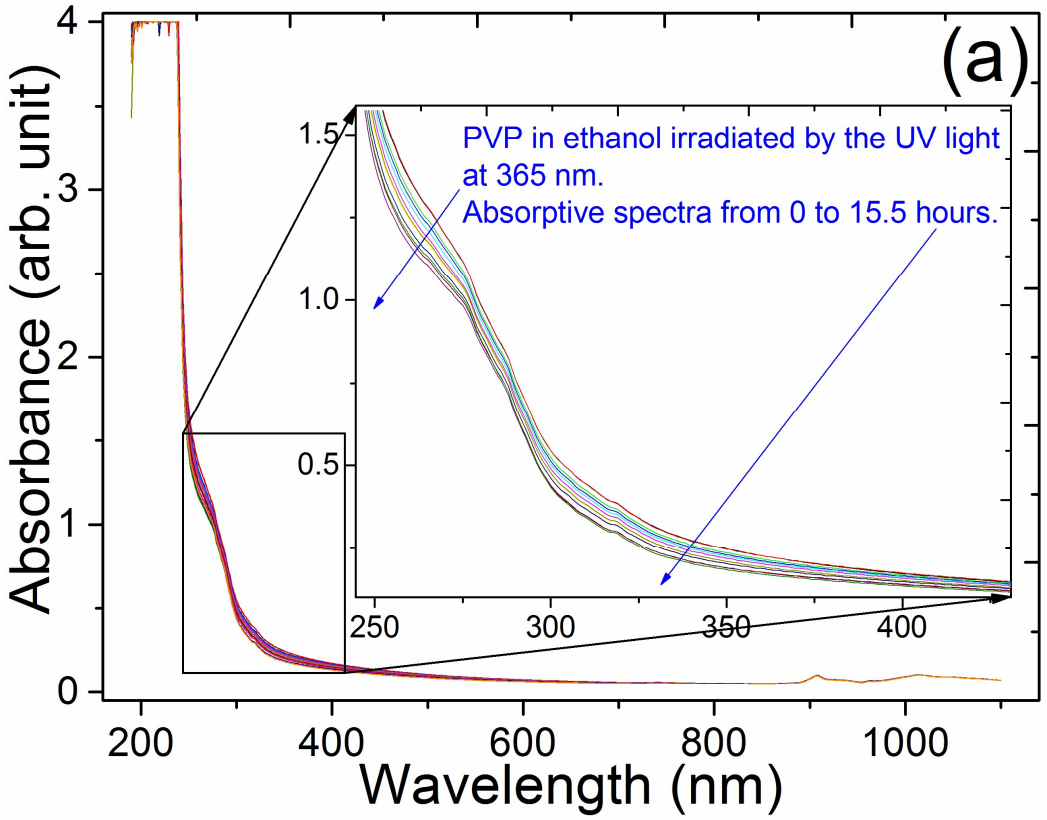

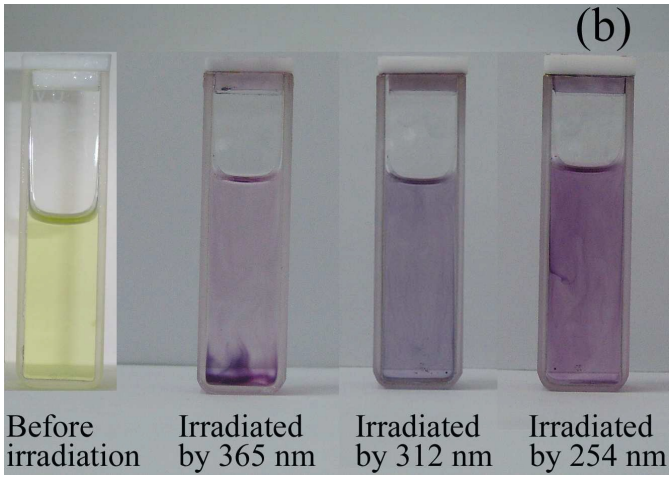

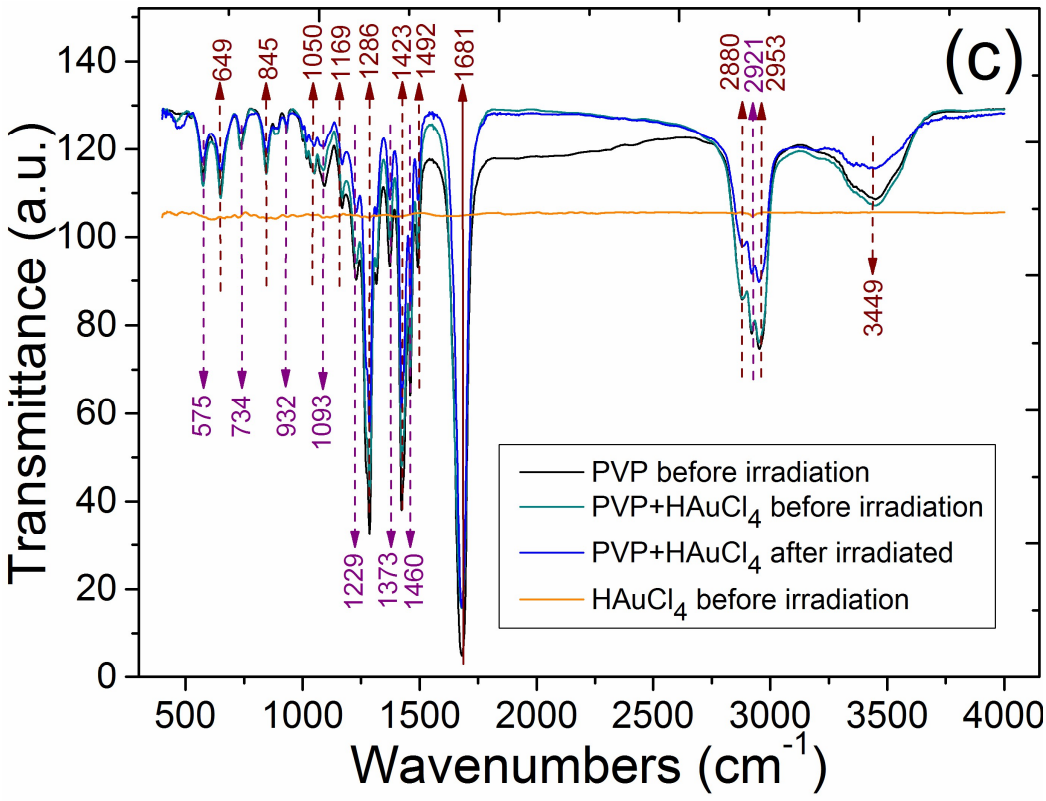

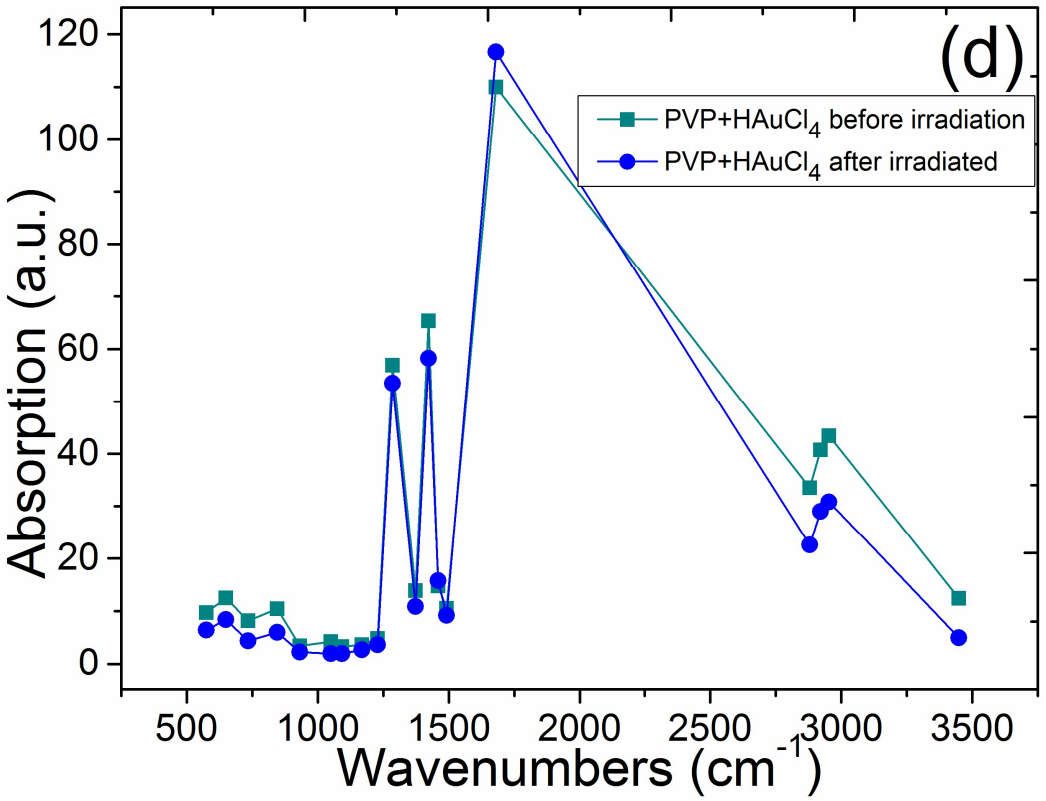

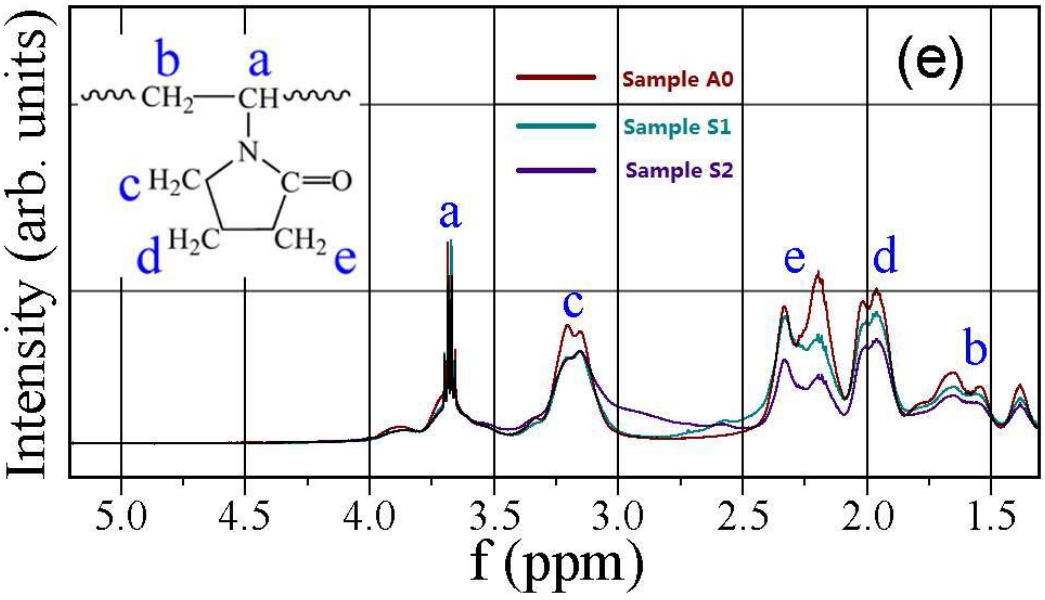

Fig. 4 (a) The time evolutions of absorption spectra of PVP (4wt %) in ethanol irradiated by UV light at 365 nm. (b) Under the respective irradiation of UV light at different wavelengths, the photos of the sample S11 shot immediately after the appearance of the pink color; the photo of the sample S11 before irradiation is also presented. (c) The FT-IR spectra of PVP, $HAuCl_4$, PVP and $HAuCl_4$ before the irradiation of UV light at 365 nm, and the FT-IR spectrum of the irradiated PVP and $HAuCl_4$. (d) The height of peaks of the FT-IR spectra of PVP, PVP and $HAuCl_4$ before and after irradiation. (e) The ^1H NMR spectra of three samples in $CDCl_3$.

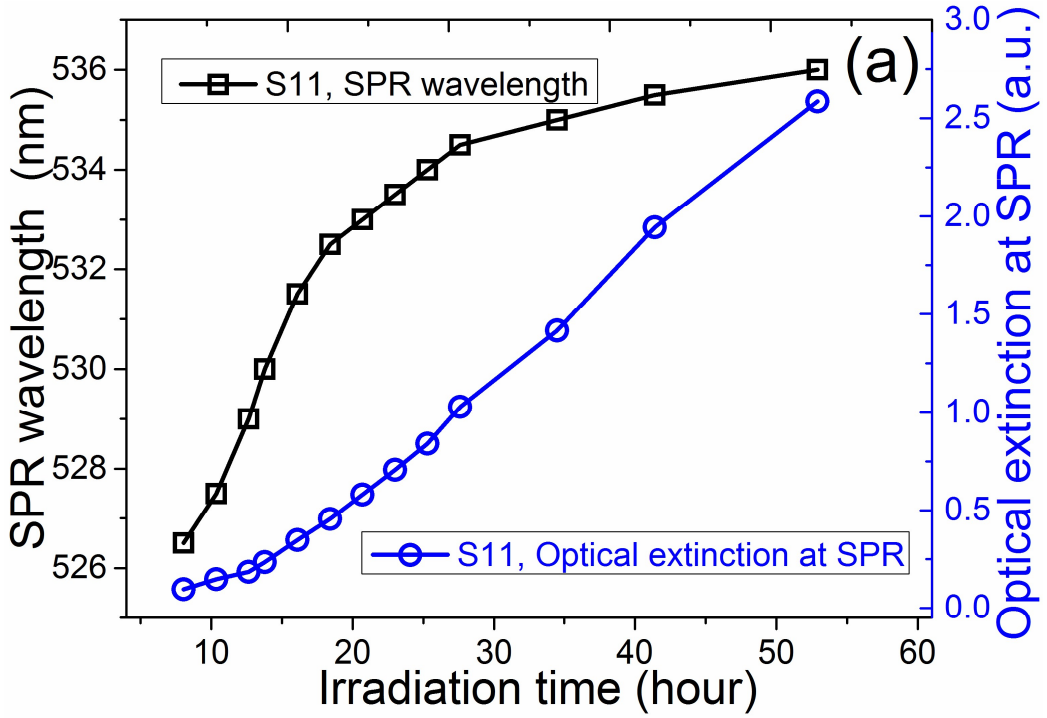

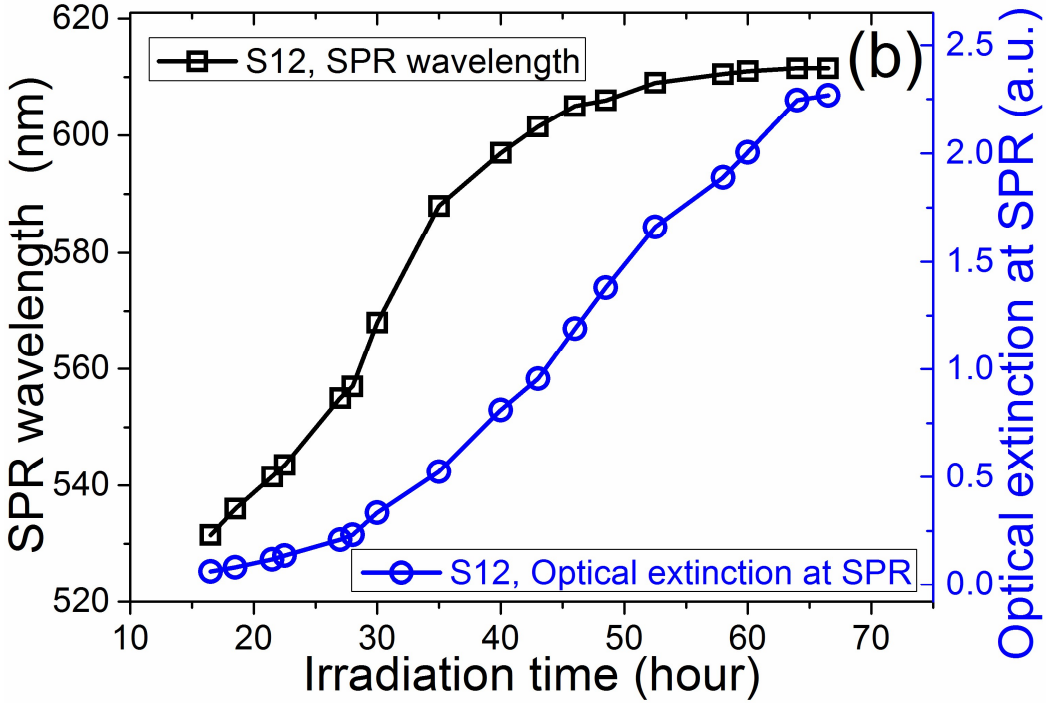

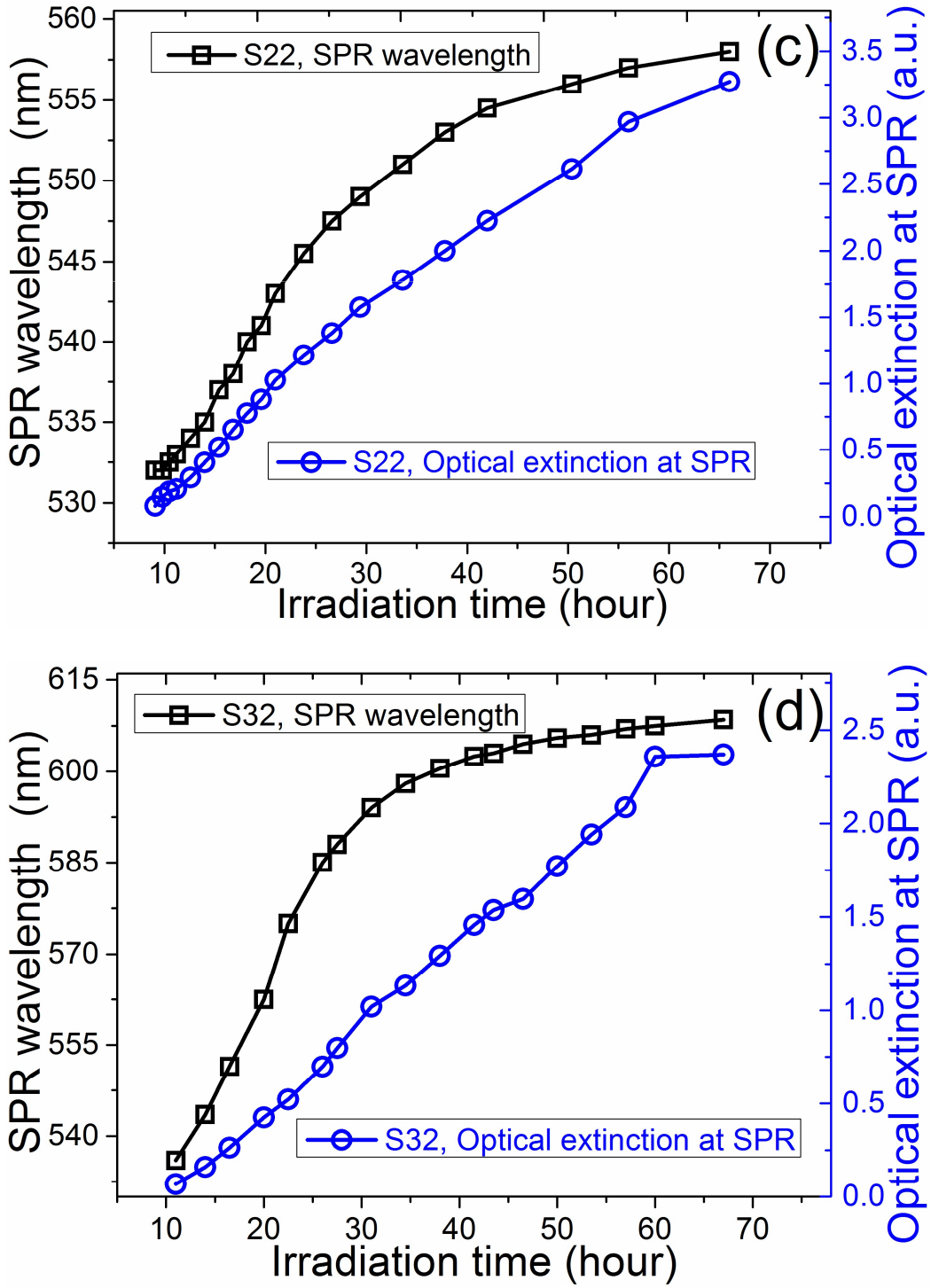

Fig. 5 The time evolutions of the SPR peak wavelength and the optical extinction intensity at the SPR peak wavelength of the as-irradiating samples, (a) S11, (b) S12, (c) S22, and (d) S32.

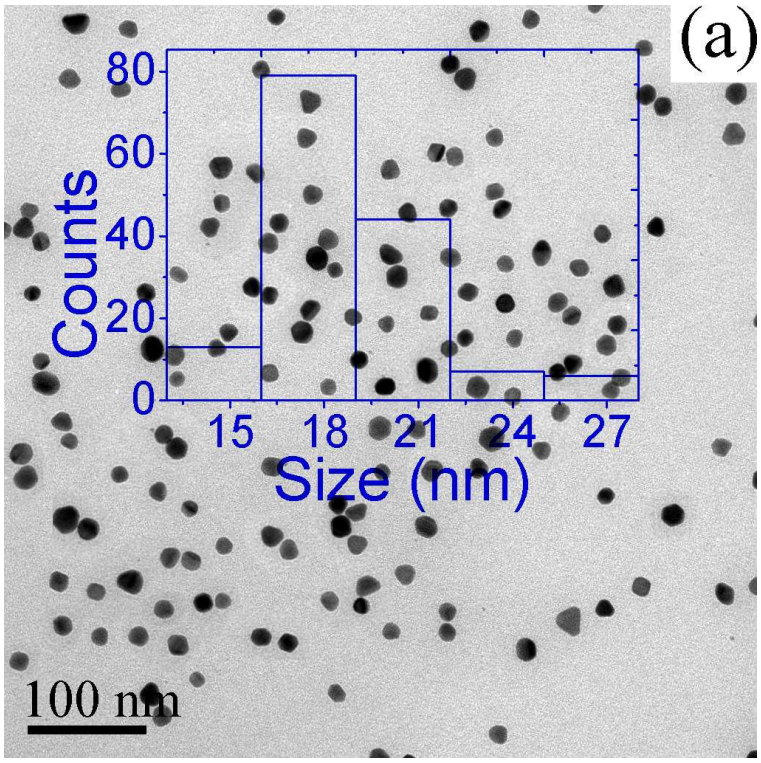

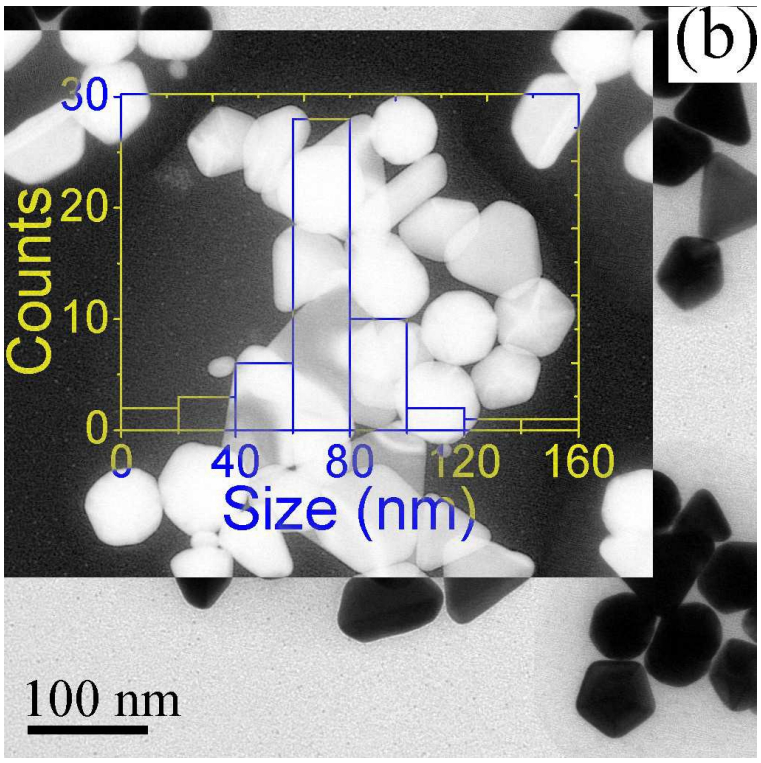

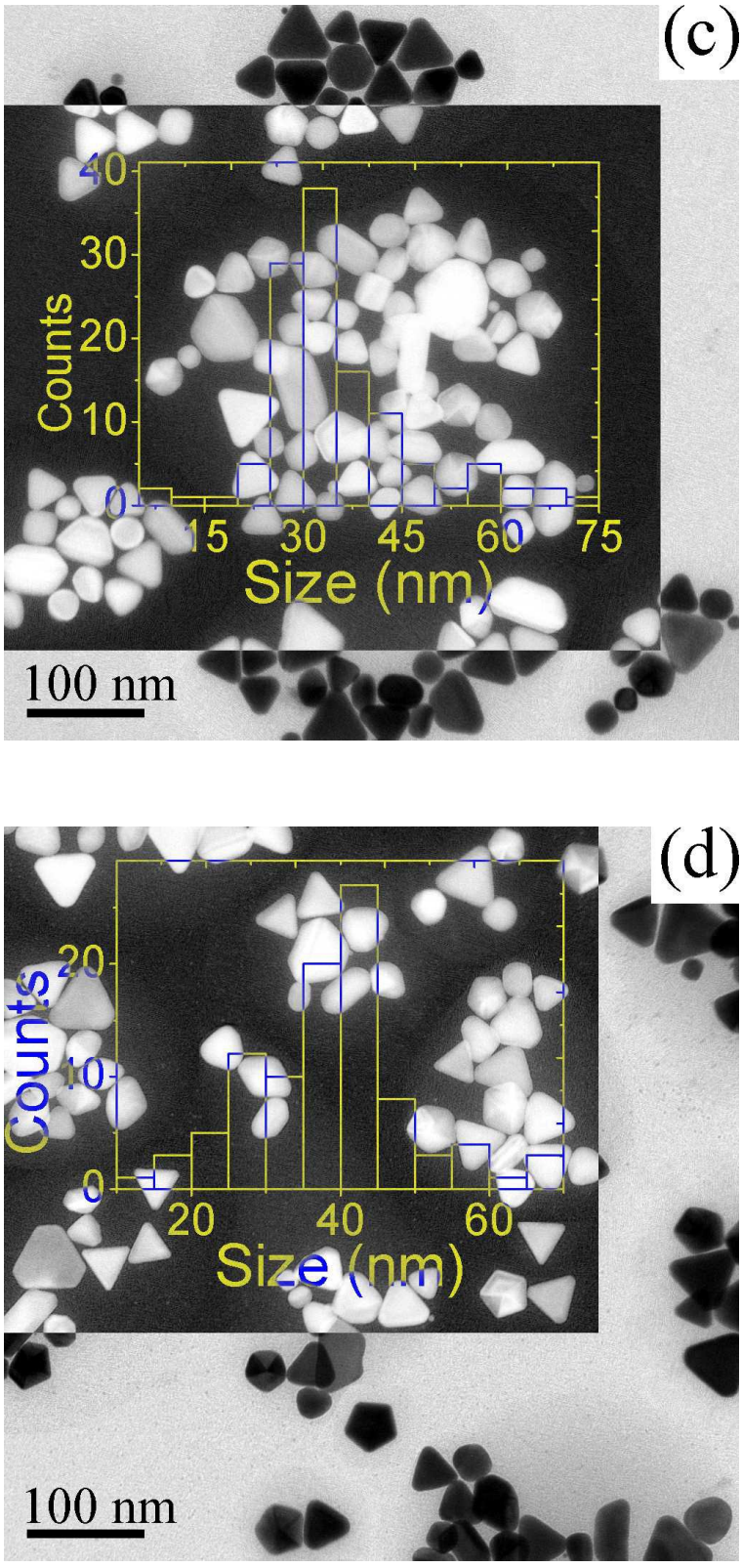

Fig. 6 The TEM images and size distribution histograms of the as-produced Au NPs in the sample 11 (a), 12 (b), 22 (c), and 32 (d).

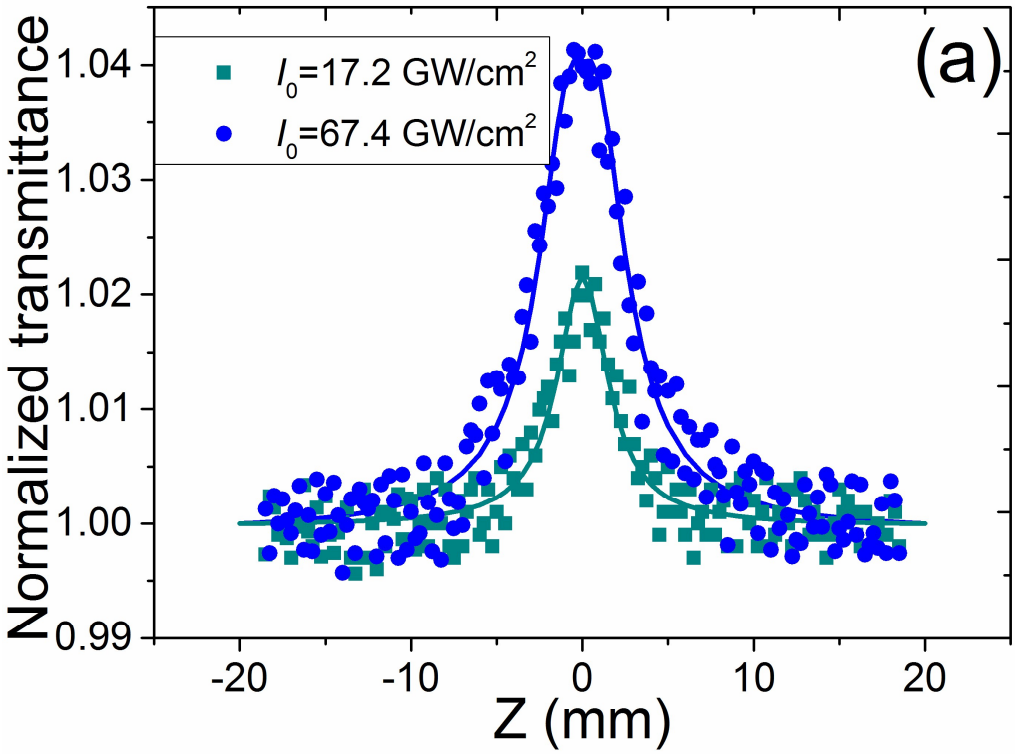

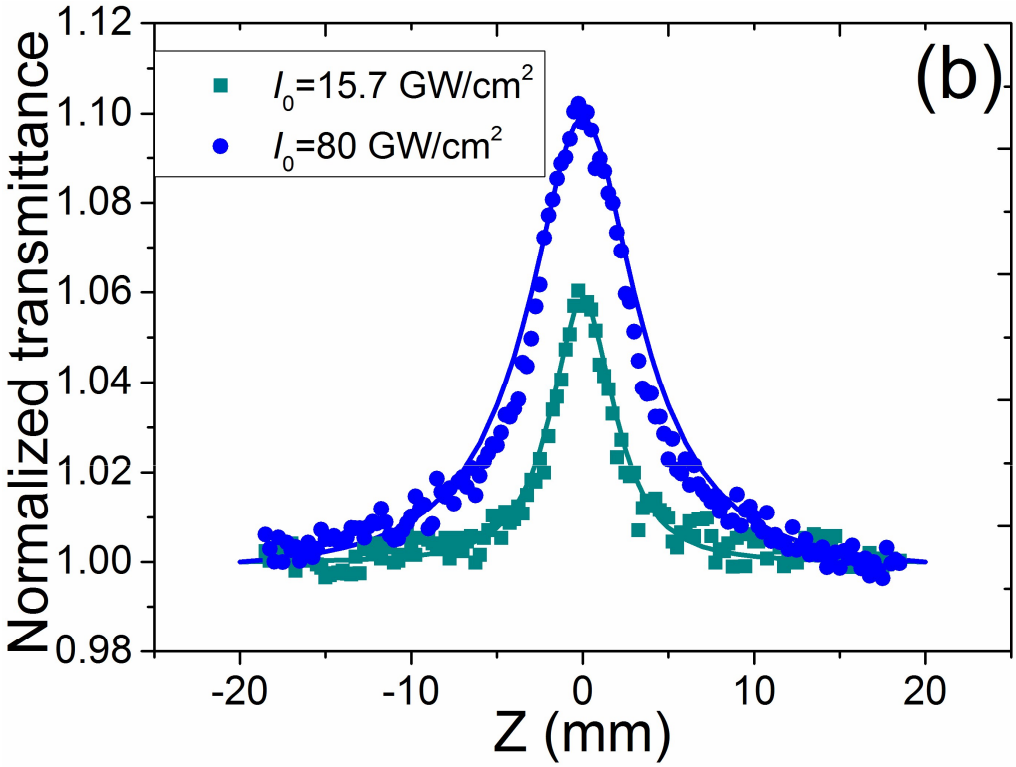

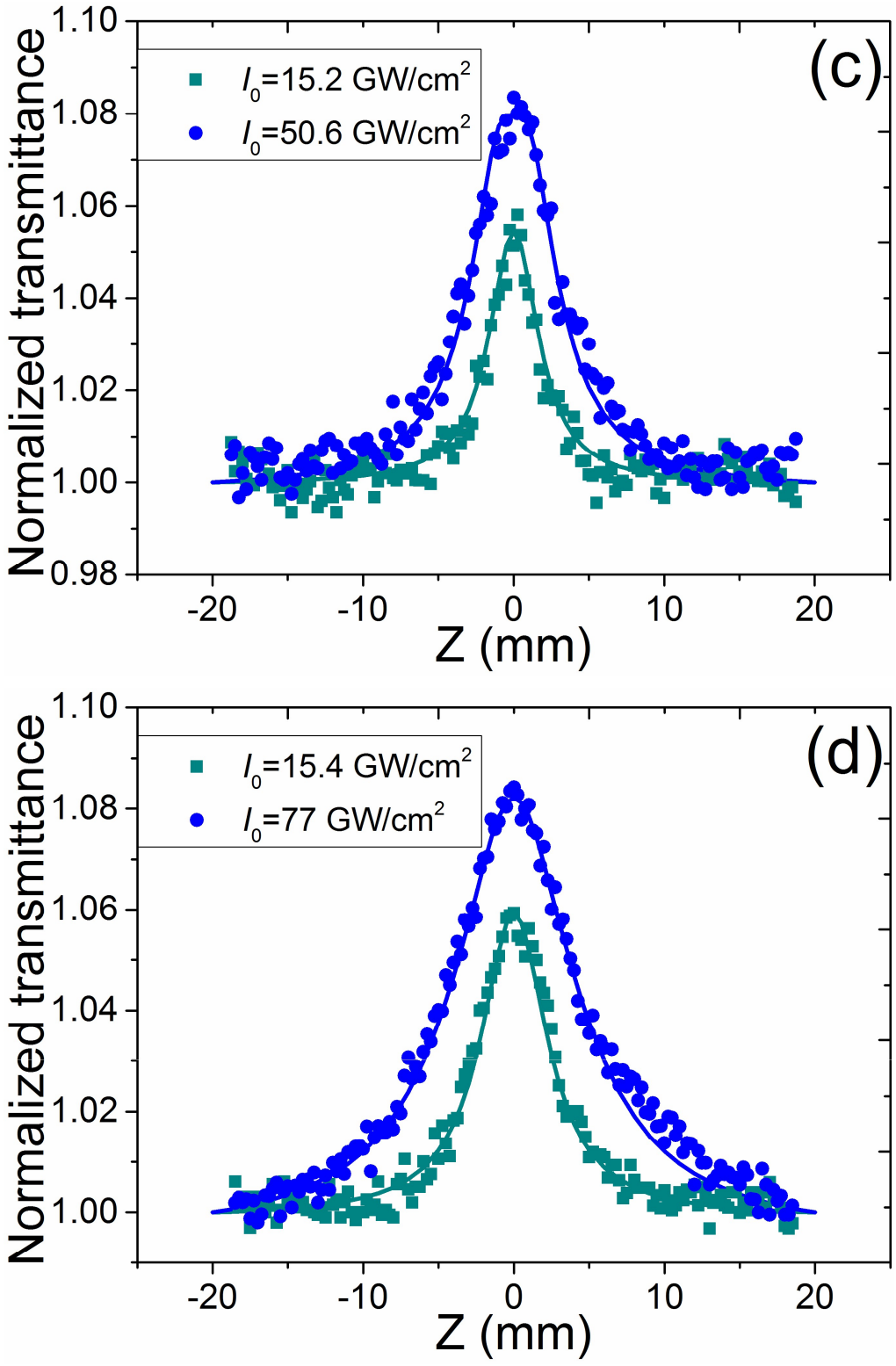

Fig. 7 The OA Z-scan experimental results of the Au nanoparticles with different mean sizes: (a) 18 nm, (b) 70 nm, (c) 32 nm, and (d) 42 nm, the peak intensity at the focus (I_0) is presented, respectively. The solid lines are theoretical fitting curves using the equations (1) to (11).

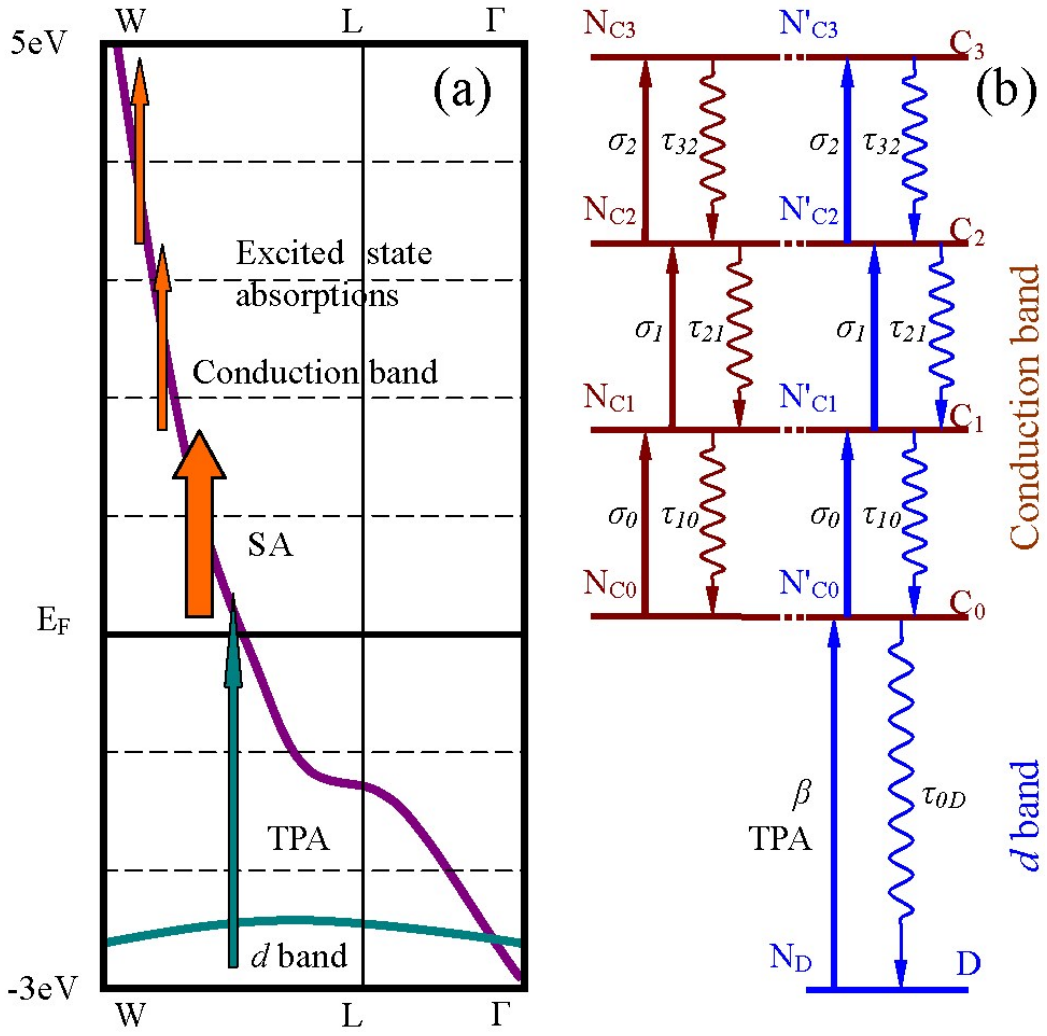

Fig. 8 Schematic diagrams of the nonlinear absorption of Au nanoparticle. (a) The energy band structures around the L point of Brillouin zone of Au nanoparticle and the nonlinear absorption. (b) Five-level model of the nonlinear absorption of Au nanoparticle.

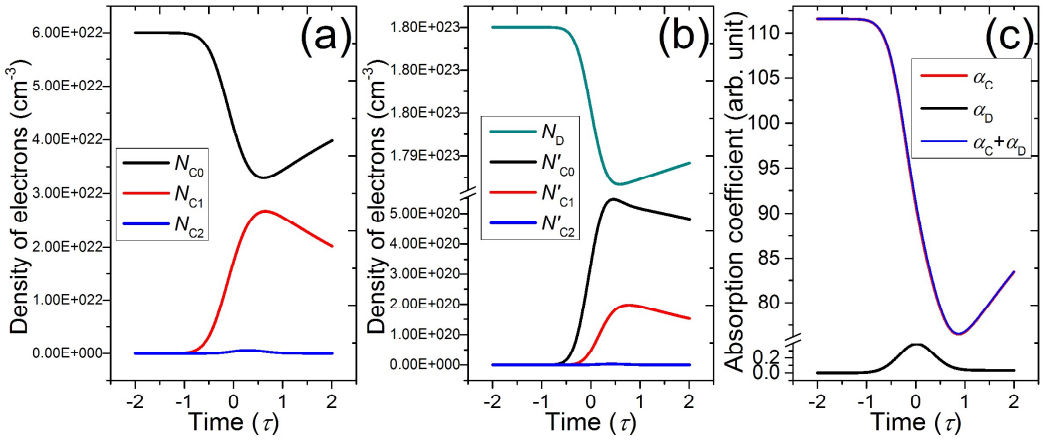

Fig 9. The changes of the number densities of the electrons and the absorption coefficients during the irradiation of a laser pulse on the sample S11. τ is the pulse duration of a laser pulse (120 fs). The intensity is 17.2 GW/cm^2. (a) The changes of the number density of the conduction band electrons in the states C_0, C_1, and C_2. (b) The changes of the number density of the *d* band electrons in the states D, C_0, C_1, and C_2. (c) The changes of the absorption coefficients of the conduction band electrons, *d* band electrons, and their sum.

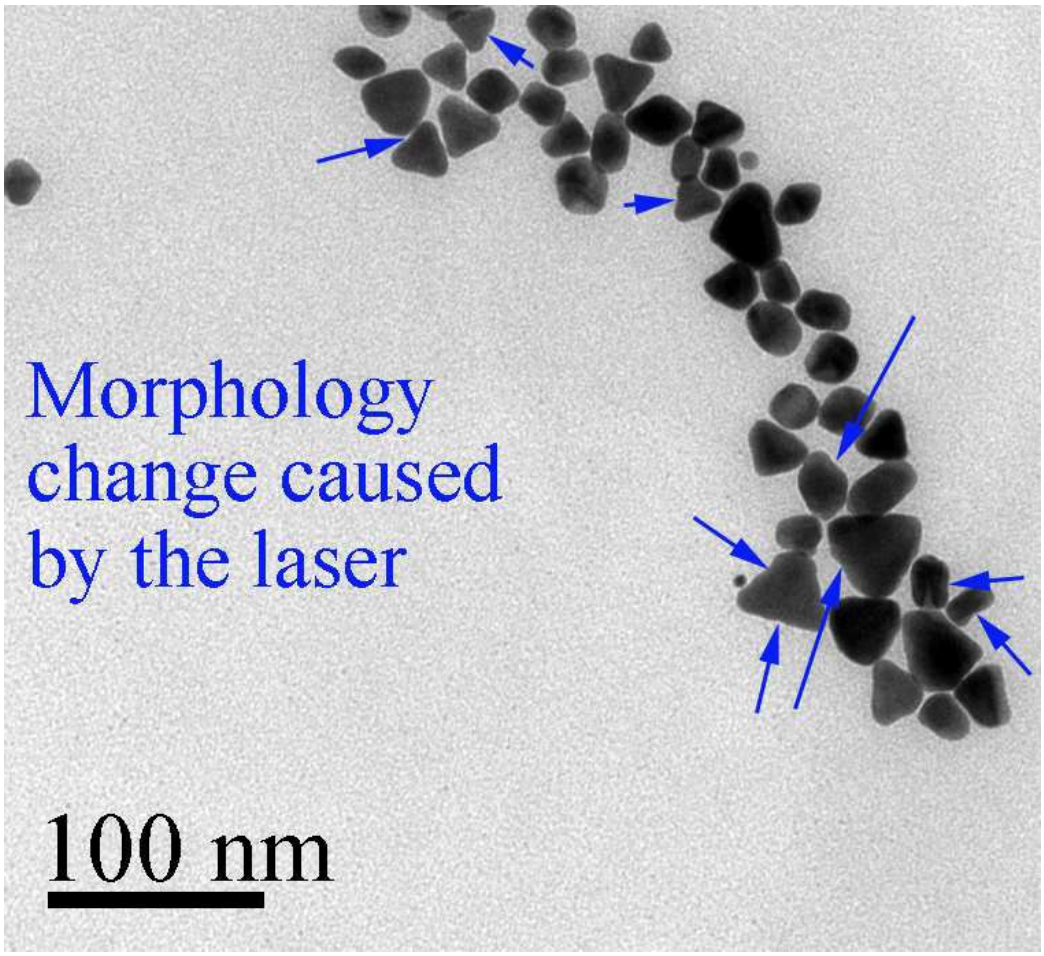

Fig. 10 The insignificant morphology change of the Au NPs in the sample 11 caused by the laser pulse irradiation, blue arrows point to the insignificant morphology change of the NPs.